RESEARCH ARTICLE SUMMARY

AGING

Spermidine activates mitochondrial trifunctional protein and improves antitumor immunity in mice

Muna Al-Habsi†, Kenji Chamoto†, Ken Matsumoto†, Norimichi Nomura†, Baihao Zhang, Yuki Sugiura, Kazuhiro Sonomura, Aprilia Maharani, Yuka Nakajima, Yibo Wu, Yayoi Nomura, Rosemary Menzies, Masaki Tajima, Koji Kitaoka, Yasuharu Haku, Sara Delghandi, Keiko Yurimoto, Fumihiko Matsuda, So Iwata, Toshihiko Ogura, Sidonia Fagarasan*, Tasuku Honjo*

INTRODUCTION: In mammals, the power of the immune system decreases with age. This is because of multiple factors, including a decrease in the output and diversity of the antigenic repertoire of T cells caused by thymus involution; changes in the cellular metabolism caused by inflammation; and defective proliferative, differentiation, or survival capacities of the immune cells. Aged individuals frequently suffer from severe infections and cancers, and often the therapies applied, including programmed cell death protein 1 (PD-1) blockade in cancer immunotherapy, are ineffective when compared with results in young patients. A biogenic polyamine, spermidine (SPD), decreases with age, and SPD supplementation was shown to improve or delay several age-related pathologies, including those of the immune system. Among the proposed mechanisms responsible for rejuvenation of the immune system by SPD were enhanced autophagy, translational activity, and mitochondrial metabolism. SPD supplementation has previously been shown to enhance the antitumor immunity in animal models. However, it remains largely unknown how SPD deficiency relates to the T cell immune suppression induced by aging.

RATIONALE: Because $CD8^+$ T cells are key players in tumor immunity, we investigated how aging would affect the metabolic and functional characteristics of $CD8^+$ T cells. We asked whether SPD insufficiency could be a factor contributing to nonresponsiveness to PD-1 antibody therapy in aged mice. We sought to characterize the $CD8^+$ T cell population changes induced by SPD supplementation in aged mice and to identify the molecular mechanisms for the SPD action.

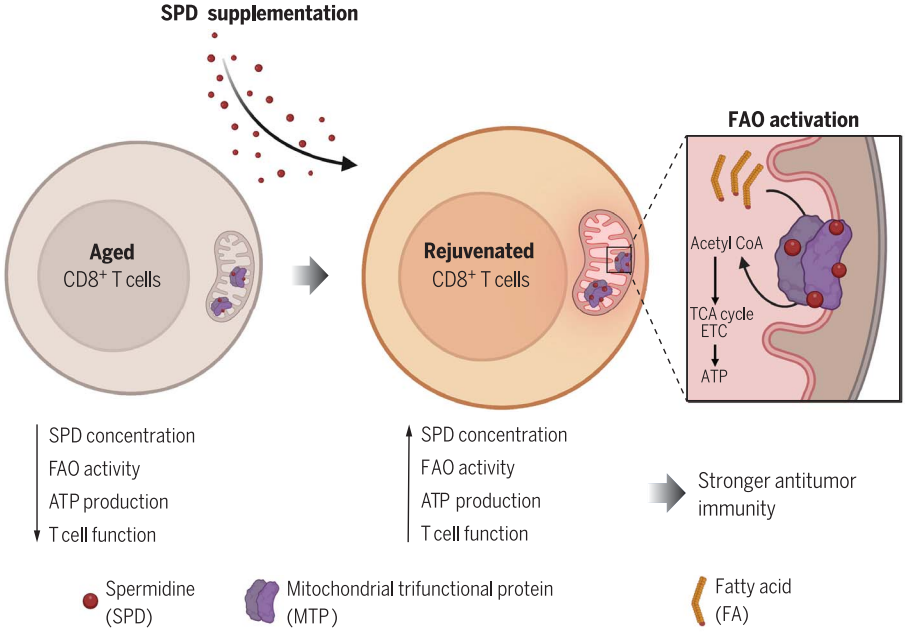

SPD binds to MTP and activates FAO in T cells. SPD directly activates MTP, which plays a central role in FAO. SPD concentration is decreased in aged T cells, leading to low FAO activity and ATP production compared with those in young T cells. SPD supplementation activates FAO in aged and young T cells, which enhances the efficacy of PD-1 blockade cancer immunotherapy. CoA, coenzyme A; TCA, tricarboxylic acid; ETC, electron transport chain. [Figure created by Biorender]

RESULTS: We found that the total and free intracellular concentrations of SPD in $CD8^+$ T cells from aged mice were about half as much as the concentrations found in young mice. Bioenergetically, aged $CD8^+$ T cells showed impaired mitochondrial activity with lower oxygen consumption rate, adenosine 5′-triphosphate (ATP) production, and fatty acid oxidation (FAO) activity compared with young $CD8^+$ T cells.

We show that SPD supplementation enhanced the antitumor activity of PD-1 blockade immunotherapy in aged mice. SPD supplementation proved to also be effective in young mice with tumors unresponsive to single anti–programmed death-ligand 1 (PD-L1) antibody therapy. SPD and anti–PD-L1 antibody combination treatment enhanced the proliferation, cytokine production, and mitochondrial ATP production of $CD8^+$ T cells in vivo. In vitro, SPD effectively enhanced mitochondrial functions and metabolized palmitate into tricarboxylic acid cycle components within 1 hour, which suggests the possibility of direct SPD binding to mitochondria-related proteins. Biochemical analysis identified SPD binding to mitochondrial trifunctional protein (MTP), which is the central enzyme of fatty acid β-oxidation. MTP is composed of α and β subunits, both of which bind SPD. Several assays using the MTP synthesized and purified from *Escherichia coli* revealed that SPD bound with strong affinity [binding affinity (dissociation constant, K_d) = 0.1 μM] and allosterically enhanced their enzymatic FAO activities. Furthermore, we found that spermine, another polyamine derived from SPD with important cellular protective functions, also directly binds to MTP and competitively inhibits FAO activity of SPD, which suggests the importance of SPD and spermine balance for FAO evaluation in aged cells. T cell–specific deletion of the MTP α subunit abolished enhancement of PD-1 blockade immunotherapy by SPD, indicating that MTP is required for SPD-dependent T cell activation.

CONCLUSION: SPD enhances FAO by directly binding and activating the MTP. SPD supplementation enhances the FAO activity and boosts the mitochondrial activities and cytotoxic functions of $CD8^+$ T cells. We provide new insights into the properties of SPD that may facilitate the development of strategies to prevent and improve outcomes of age-related immune pathologies and combat unresponsiveness to PD-1 blockade therapy in cancers, regardless of age. ■

The list of author affiliations is available in the full article online.
*Corresponding author. Email: honjo@mfour.med.kyoto-u.ac.jp (T.H.); sidonia.fagarasan@riken.jp (S.F.)
†These authors contributed equally to this work.
Cite this article as M. Al-Habsi *et al.*, *Science* **378**, eabj3510 (2022). DOI: 10.1126/science.abj3510

READ THE FULL ARTICLE AT
https://doi.org/10.1126/science.abj3510

RESEARCH ARTICLE

AGING

Spermidine activates mitochondrial trifunctional protein and improves antitumor immunity in mice

Muna Al-Habsi[1,2,3]†, Kenji Chamoto[1]†, Ken Matsumoto[4]†, Norimichi Nomura[5]†, Baihao Zhang[6], Yuki Sugiura[7], Kazuhiro Sonomura[8,9], Aprilia Maharani[1], Yuka Nakajima[1], Yibo Wu[10,11], Yayoi Nomura[5], Rosemary Menzies[1], Masaki Tajima[3], Koji Kitaoka[1], Yasuharu Haku[1], Sara Delghandi[1], Keiko Yurimoto[1], Fumihiko Matsuda[8], So Iwata[5], Toshihiko Ogura[4], Sidonia Fagarasan[3,6]*, Tasuku Honjo[1]*

Spermidine (SPD) delays age-related pathologies in various organisms. SPD supplementation overcame the impaired immunotherapy against tumors in aged mice by increasing mitochondrial function and activating CD8$^+$ T cells. Treatment of naïve CD8$^+$ T cells with SPD acutely enhanced fatty acid oxidation. SPD conjugated to beads bound to the mitochondrial trifunctional protein (MTP). In the MTP complex, synthesized and purified from *Escherichia coli*, SPD bound to the α and β subunits of MTP with strong affinity and allosterically enhanced their enzymatic activities. T cell–specific deletion of the MTP α subunit abolished enhancement of programmed cell death protein 1 (PD-1) blockade immunotherapy by SPD, indicating that MTP is required for SPD-dependent T cell activation.

Aged animals undergo changes in metabolic pathways related to sugars, fatty acids, amino acids, and mitochondrial functions including redox homeostasis (*1*–*3*). For example, increased amounts of free fatty acids, decreased long-chain acylcarnitines, and decreased abundance of various amino acids such as proline and tyrosine occur in the plasma of aged mice (*1*). Abundance of spermidine (SPD), a natural polyamine, decreases with aging, and dietary supplementation of SPD not only prolongs the life span of diverse organisms, such as yeast, worms, flies, mice, and humans, but also improves age-related dysfunction of cardiac, nervous, hepatic, and immune systems (*4*). In mice, SPD administration induces metabolic changes in various tissues, including muscle and the liver, that resemble changes induced by fasting or the administration of caloric restriction mimetics, such as metformin (*4*). SPD induces autophagy in multiple cells and tissues (*4*, *5*). In the immune systems of aged mice, antitumor immunity is defective because of the impaired activation and differentiation of effector and memory (CD44^{high} CD62L^{low}) T cells (*6*). SPD improves the generation and function of memory T lymphocytes, similarly to other autophagy inducers such as rapamycin or metformin (*7*, *8*). Because the generation and maintenance of memory T cells depend on fatty acid oxidation (FAO), we wondered whether SPD might also regulate FAO (*9*, *10*).

Biochemical mechanisms have been proposed by which SPD restores age-induced damage. SPD inhibits protein acetylation by direct inhibition of protein acetyl transferases, such as EP300, and may affect autophagy by epigenetic regulation (*11*). SPD is a substrate for the hypusination reaction of eukaryotic elongation factor 5A (eIF5A), which is critical to cell proliferation because it activates protein synthesis and mitochondrial function (*12*, *13*). Epigenetic changes caused by SPD are also attributed to the SPD-hypusine axis (*14*). However, several SPD analogs that cannot provide the hypusine moiety also rescue acute growth arrest caused by SPD depletion, which suggests that there may be other mechanisms of SPD function (*15*).

SPD restores the efficacy of programmed cell death protein 1 (PD-1) blockade therapy in aged mice through the activation of effector and mitochondrial function in CD8$^+$ T cells

We confirmed that serum concentrations of SPD—but not those of other polyamines—were significantly decreased in aged mice (>12 months) (Fig. 1A) (*4*, *5*). Furthermore, intracellular total and free SPD concentrations in naïve CD8$^+$ T cells from old mice were about half as much as the concentrations found in young mice (Fig. 1B). We therefore wondered whether SPD insufficiency could be a factor contributing to nonresponsiveness to programmed death-ligand 1 (PD-L1) monoclonal antibody (mAb) therapy in aged mice (*6*). SPD supplementation significantly improved the antitumor effect of PD-L1 mAb treatment and prolonged the survival of aged mice (Fig. 1C). SPD alone had no antitumor effect (Fig. 1C). Flow cytometric analysis revealed that the frequency and numbers of CD8$^+$ T cells in tumor-infiltrating lymphocytes (TILs) were significantly increased in aged mice that received the combination therapy with PD-L1 mAb and SPD (Fig. 1, D and E). SPD combination therapy increased the abundance of PD-1$^-$ Tim3$^-$ nonexhausted effector CD8$^+$ T cells and increased the expression of cytotoxicity marker granzyme B (Fig. 1, F and G).

SPD supplementation also enhanced antitumor activity and prolonged survival in young mice, in which PD-L1 mAb treatment was partially effective and SPD alone was ineffective (fig. S1A). As in old mice, SPD combination therapy increased frequencies and numbers of CD8$^+$ T cells exhibiting a nonexhausted PD-1$^-$ Tim3$^-$ phenotype and producing more granzyme B (fig. S1, B to E). Treatment of young mice with SPD alone reportedly increased the abundance of regulatory T cells (T_{regs}) and inhibitory arginase-1 (Arg1$^+$) M2 macrophages (*16*, *17*). However, the abundance of Foxp3$^+$ regulatory cells and myeloid cells, including Arg1$^+$ macrophages (M2) or major histocompatibility complex (MHC) II$^+$ macrophage (M1), was not significantly changed by SPD treatment in our mice (fig. S1, F and G). This discrepancy might be related to the SPD amounts used, which were 15- to 25-fold higher than those that we used (30 mM in drinking water and 50 mg/kg for effects on T_{regs} and M2 macrophages, respectively, versus 200 μl of 1.4 mM intraperitoneal injection = 2 mg/kg in our case). The abundance of other cells with potential antitumor activity, such as natural killer (NK) cells, was not changed by the SPD treatment (fig. S1H). In other tumor models, SPD also enhanced the antitumor activity of PD-L1 mAb against unresponsive tumor cells, such as colorectal carcinoma (CT26) in BALB/c mice and Lewis lung carcinoma (LLC) in C57BL/6 mice (fig. S1I).

PD-1 blockade increases the number of activated effector T cells but reduces their longevity and promotes exhaustion through the glycolysis pathway (*18*–*20*). To know the effect of SPD on T cell differentiation in vivo, we assessed changes in subpopulations of CD8$^+$ T cells in draining lymph nodes (DLNs). SPD in combination with PD-1 blockade increased

[1]Division of Immunology and Genomic Medicine, Center for Cancer Immunotherapy and Immunobiology, Graduate School of Medicine, Kyoto University, Kyoto, Japan. [2]National Genetic Center, Ministry of Health, Muscat, Oman. [3]Division of Integrated High-Order Regulatory Systems, Center for Cancer Immunotherapy and Immunobiology, Graduate School of Medicine, Kyoto University, Kyoto, Japan. [4]Department of Developmental Neurobiology, Institute of Development, Aging and Cancer, Tohoku University, Miyagi, Japan. [5]Department of Cell Biology, Graduate School of Medicine, Kyoto University, Kyoto, Japan. [6]Laboratory for Mucosal Immunity, Center for Integrative Medical Sciences, RIKEN Yokohama Institute, Yokohama, Japan. [7]Department of Biochemistry, Keio University, Tokyo, Japan. [8]Center for Genomic Medicine, Graduate School of Medicine, Kyoto University, Kyoto, Japan. [9]Life Science Research Center, Technology Research Laboratory, Shimadzu Corporation, Kyoto, Japan. [10]YCI Laboratory for Next-Generation Proteomics, Center for Integrative Medical Sciences, RIKEN Yokohama Institute, Yokohama, Japan. [11]Chemical Biology Mass Spectrometry Platform, Faculty of Science, University of Geneva, Geneva, Switzerland.
*Corresponding author. Email: honjo@mfour.med.kyoto-u.ac.jp (T.H.); sidonia.fagarasan@riken.jp (S.F.)
†These authors contributed equally to this work.

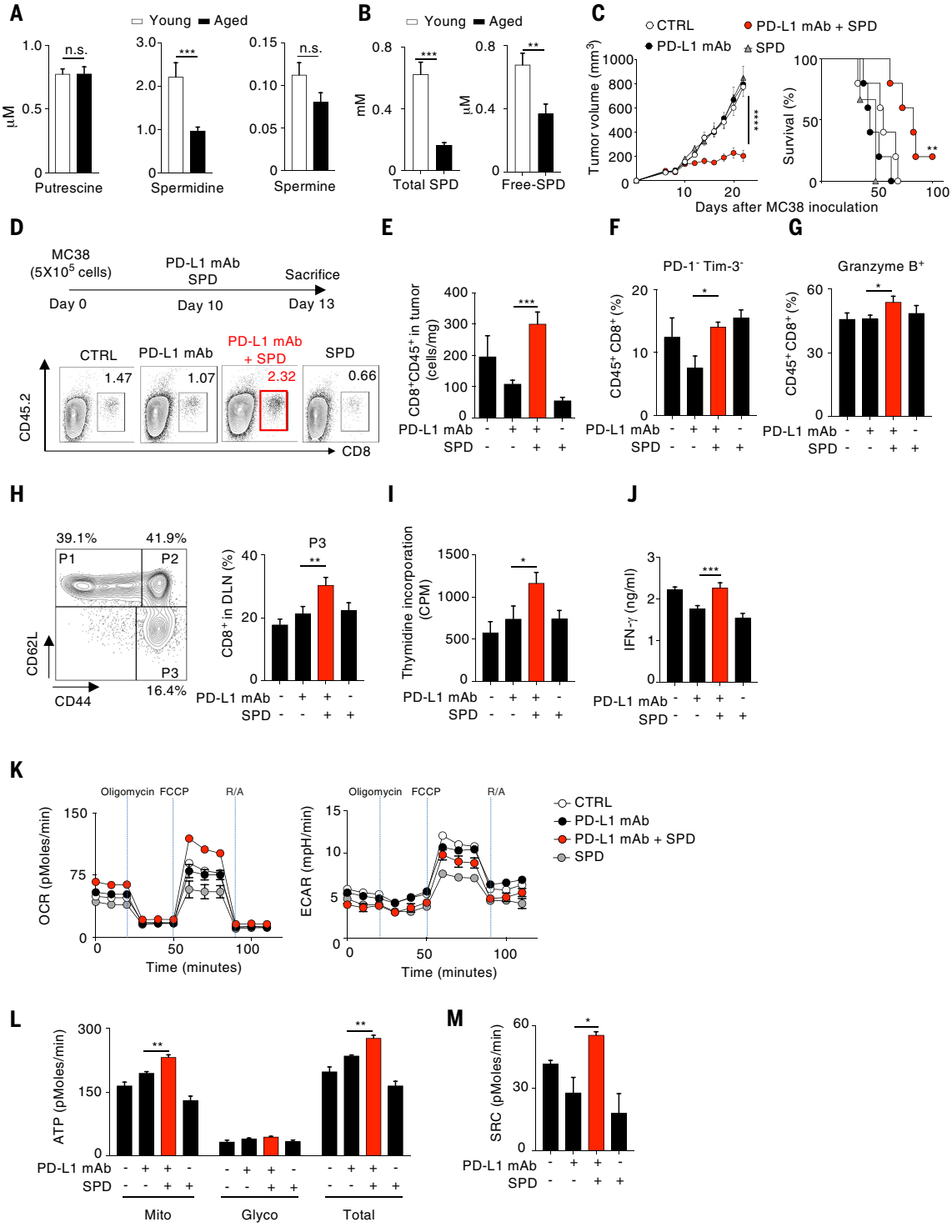

Fig. 1. SPD combination improves antitumor activity of PD-1 blockade therapy and enhances mitochondrial function of CD8$^+$ T cells. (**A**) Quantification of polyamines in sera from young (1 to 3 months, n = 31 mice) and aged (>1 year, n = 30) mice using mass spectrometry. (**B**) Total and free SPD levels in naïve CD8$^+$ T cells from young [n = 12 mice (total SPD) or 10 mice (free SPD)] and aged (n = 8) mice. (**C**) MC38 tumor–bearing aged mice were intraperitonially treated with PD-L1 mAb and/or SPD (2 mg/kg) every 5 days from day 10. Tumor growth and survival curve of mice are shown from pooled mice [n = 3 mice (SPD alone group) or 5 mice (the other groups)] (log-rank for survival curve). (D to G) Tumor-infiltrating CD8$^+$ T cells were gated and analyzed on day 13 after MC38 inoculation. CTRL, control. (**D** and **E**) Flow cytometry frequencies and quantification (cells per milligram) of tumor-infiltrating CD8$^+$ T cells (n = 6 mice). (**F**) Frequencies of PD-1$^-$ Tim-3$^-$ nonexhausted CD8$^+$ T cells [n = 9 mice (control or SPD group) or 7 mice (the other groups)]. (**G**) Frequencies of granzyme B–producing CD8$^+$ T cells in tumor without stimulation [n = 7 mice (control or SPD group) or 8 mice (the other groups)]. (**H**) A representative flow cytometry profile of CD8$^+$ gated T cell subpopulations (P1 = naïve, P2 = memory, and P3 = effector) in the tumor DLNs (left) and frequencies of P3 cells (right) (n = 5 mice). (**I** and **J**) Thymidine incorporation (n = 5 technical replicates) (I) and IFN-γ production (n = 6 technical replicates) (J) of total DLN CD8$^+$ T cells pooled from five mice, after restimulation with anti-CD3 and anti-CD28 coated beads. CPM, counts per minute. (**K**) Real-time OCR (left) and ECAR (right) of total DLN CD8$^+$ T cells pooled from five mice per group, as assessed by Seahorse assay (n = 3 technical replicates). R/A, rotenone + antimycin A. (**L** and **M**) ATP production rate (L) and SRC (M) from data in (K), calculated as indicated in fig. S2, A and B. Data are the means ± SEMs [(C) and (K)] or + SEMs [(A), (B), (E) to (J), (L), and (M)]. P values were determined using unpaired two-tailed Student's t tests [(A) and (B)], two-way ANOVA [(C) on day 22], or one-way ANOVA [(E) to (J), (L), and (M)] with selected column comparison between PD-L1 mAb and SPD combination group. *P < 0.05; **P < 0.01; ***P < 0.001; n.s, not significant. All data are representative of three or more experiments.

the numbers of effector and memory (P3) $CD8^+$ T cells, whereas single treatment with PD-L1 mAb or SPD marginally increased the P3 $CD8^+$ T cells in the DLNs of aged mice (Fig. 1H). $CD8^+$ T cells isolated from the DLNs of tumor-bearing aged mice treated with the PD-L1 mAb and SPD combination showed higher proliferation capacity and augmented interferon-γ (IFN-γ) production compared with those treated with a single therapy or with control mice (Fig. 1, I and J). Because mitochondrial activity of T cells is associated with antitumor activity (*19*, *21*), we used the Seahorse assay system to assess the bioenergetics in the $CD8^+$ T cells in DLNs from tumor-bearing mice treated with or without SPD combination. We measured oxygen consumption rate (OCR) and extracellular acidification rate (ECAR)—which reflect oxidative phosphorylation (OXPHOS) and glycolysis, respectively—at the basal state and after sequential addition of oligomycin [blocking OXPHOS-dependent adenosine 5′-triphosphate (ATP) synthesis], carbonyl cyanide-4 (trifluoromethoxy) phenylhydrazone (FCCP) (uncoupling the ATP synthesis from the electron transport chain), and rotenone plus antimycin A (blocking electron transport complexes I and III, respectively) (Fig. 1K) (*22*). Mitochondria- and glycolysis-derived ATP production were calculated on the basis of the change in OCR and ECAR, respectively, caused by oligomycin injection (fig. S2, A and B). Compared with the $CD8^+$ T cells from mice receiving a single or no therapy, the $CD8^+$ T cells from the DLNs of aged mice receiving SPD combination therapy exhibited enhanced OXPHOS and mitochondrial ATP production (Fig. 1, K and L). SPD combination treatment also enhanced the spare respiratory capacity (SRC), which is represented by the OCR uncoupled from ATP production and reflects the mitochondrial metabolic potential linked to longevity and memory formation of T cells (fig. S2A and Fig. 1M) (*23*, *24*). Similar phenotypes and bioenergetic profiles were obtained with $CD8^+$ T cells isolated from the DLNs of MC38 tumor–bearing young mice (fig. S3, A to F). Further evidence of mitochondrial activation in vivo was obtained by proteomics analysis of sorted $CD8^+$ T cells from the DLNs of young mice, which showed a significant increase in abundance of many proteins by SPD combination treatment compared with treatment with PD-L1 mAb alone (fig. S3G). Among the 95 proteins that increased in abundance, 35 were related to OXPHOS, including the glycolysis-derived reduced form of nicotinamide adenine dinucleotide (NADH) dehydrogenase [ubiquinone] 1 α subunits (a component of complex-1), some cytochromes, and adenosine triphosphatases (ATPases) (fig. S3, H to J). These data indicate that SPD enhances the effectiveness of PD-1 blockade immunotherapy by preventing exhaustion and boosting the effector functions of $CD8^+$ T cells through the activation of mitochondrial metabolism.

SPD enhances mitochondrial FAO activity in $CD8^+$ T cells in 1 hour

Because SPD administration increased the SRC of $CD8^+$ T cells in vivo, which is associated with FAO activity (*10*, *23*, *24*), we next investigated the effect of SPD on FAO in vitro by using etomoxir, a specific inhibitor of carnitine palmitoyltransferase 1a (CPT1a) (*25*). To examine the effects of SPD on FAO activity, we measured bioenergetic states of naïve $CD8^+$ T cells from old mice after in vitro stimulation with anti-CD3 and -CD28 mAb-coated beads in the presence or absence of SPD and etomoxir. After 44 hours, SPD treatment increased ATP production and SRC by enhancing the mitochondrial and glycolytic activities (Fig. 2, A and B). SPD appeared to enhance OCR through FAO in stimulated $CD8^+$ T cells because SPD effects were inhibited by etomoxir (Fig. 2, A and B). FAO-dependent OCR coupled with ATP production (calculated as presented in fig. S2C) was increased by SPD (Fig. 2C). Mitochondrial bioenergetics, such as OCR, ATP production, and SRC, declined in aged $CD8^+$ T cells compared with $CD8^+$ T cells isolated from young mice (Fig. 2, D to F). In the absence of exogenous SPD, FAO activity in aged $CD8^+$ T cells was significantly decreased compared with that in young $CD8^+$ T cells, consistent with decreased SPD abundance in aged $CD8^+$ T cells (Fig. 2G and Fig. 1B). The addition of SPD restored proliferation in aged $CD8^+$ T cells (Fig. 2H). Because SPD combination treatment was effective not only in old but also in young mice (Fig. 1C and fig. S1A), we investigated whether SPD could boost the bioenergetics of $CD8^+$ T cells sorted from young mice. The addition of exogeneous SPD to $CD8^+$ T cell cultures from young mice also boosted the ATP production and FAO activity to a degree comparable to those changes observed in cultures with $CD8^+$ T cells isolated from old mice (fig. S4, A to C).

We examined the possibility that SPD directly stimulates FAO in mitochondria, which increases the SRC required for T cells' longevity and memory formation (*10*, *24*). Naïve $CD8^+$ T cells sorted from old mice and stimulated for only 1 hour with anti-CD3 and -CD28 mAb-coated beads in the presence of SPD showed enhanced mitochondrial and glycolytic activities and increased ATP production as well as SRC (Fig. 2, I to L). Similar results were obtained with naïve $CD8^+$ T cells isolated from young mice 1 hour after stimulation (fig. S4, D to G).

We further confirmed the immediate effect of SPD on FAO by several approaches using naïve $CD8^+$ T cells isolated from young mice. In the real-time Seahorse system in which SPD was injected in situ, SPD quickly increased the OCR of $CD8^+$ T cells stimulated with immobilized anti-CD3 and -CD28 mAb, and etomoxir cancelled enhancement of OCR (fig. S4H). SPD enhancement of OCR was observed in the media containing palmitate without glucose (fig. S4I). We further examined whether SPD directly facilitates FAO by analyzing the generation of energy metabolism–related compounds from ^{13}C-labeled palmitate in sorted naïve $CD8^+$ T cells, activated in vitro in the presence or absence of SPD. Just 1 hour after SPD stimulation, the incorporation of ^{13}C in tricarboxylic acid (TCA) cycle–associated metabolites, such as citrate, malate, isocitrate, and fumarate, was significantly enhanced by SPD (fig. S4, J and K). Although SPD exerted similar effects on effector and memory $CD44^+$ $CD8^+$ T cell populations at 44 hours, they were not as sizeable after 1 hour of stimulation (fig. S5, A and B). This suggests that the mechanism we describe is more prominent in naïve $CD8^+$ T cells.

SPD directly binds a central enzyme of FAO, mitochondrial trifunctional protein (MTP)

SPD enhances mitochondrial respiration through hypusination of translation factor eIF5A (*13*, *26*). Therefore, we tested whether a similar mechanism functions in boosting mitochondrial metabolism in $CD8^+$ T cells. GC7, a hypusination inhibitor that acts by blocking the deoxyhypusine synthase, the rate-limiting enzyme for eIF5A hypusination, did not inhibit acute (1 hour) mitochondrial activation of $CD8^+$ T cells by SPD (fig. S6A). In the later phase (44 hours), however, GC7 significantly decreased mitochondrial ATP production, as it dampened OXPHOS but not glycolytic activity (fig. S6B). Although SPD enhances autophagy and mitophagy activity, we did not observe changes in mitochondrial morphology or accumulation of autophagy-related proteins in 1 hour after stimulation (fig. S6, C and D). Thus, the synthesis of mitochondrial proteins and autophagic activity might be later effects of mitochondrial metabolism. Acute enhancement of mitochondrial respiration by SPD appears to be dependent on its direct activation of FAO.

To explore whether SPD directly activates FAO in mitochondria, we examined whether SPD bound to any mitochondrial components. We used nanomagnetic particles coated with SPD [SPD-coated ferrite-glycidyl methacrylate (FG) beads] to isolate SPD-binding proteins from the cell lysates of HeLa and eluted bound proteins in a high-salt buffer containing 2 or 4 mM SPD (Fig. 3A). We then separated the eluted proteins by electrophoresis and subjected the SPD-eluted bands A, B, and C to mass spectrometry (MS) (Fig. 3A). Among the proteins constantly detected in all three bands, we identified hydroxyl coenzyme A (CoA) dehydrogenase subunits α and β (HADHA and HADHB, respectively) that make up the MTP

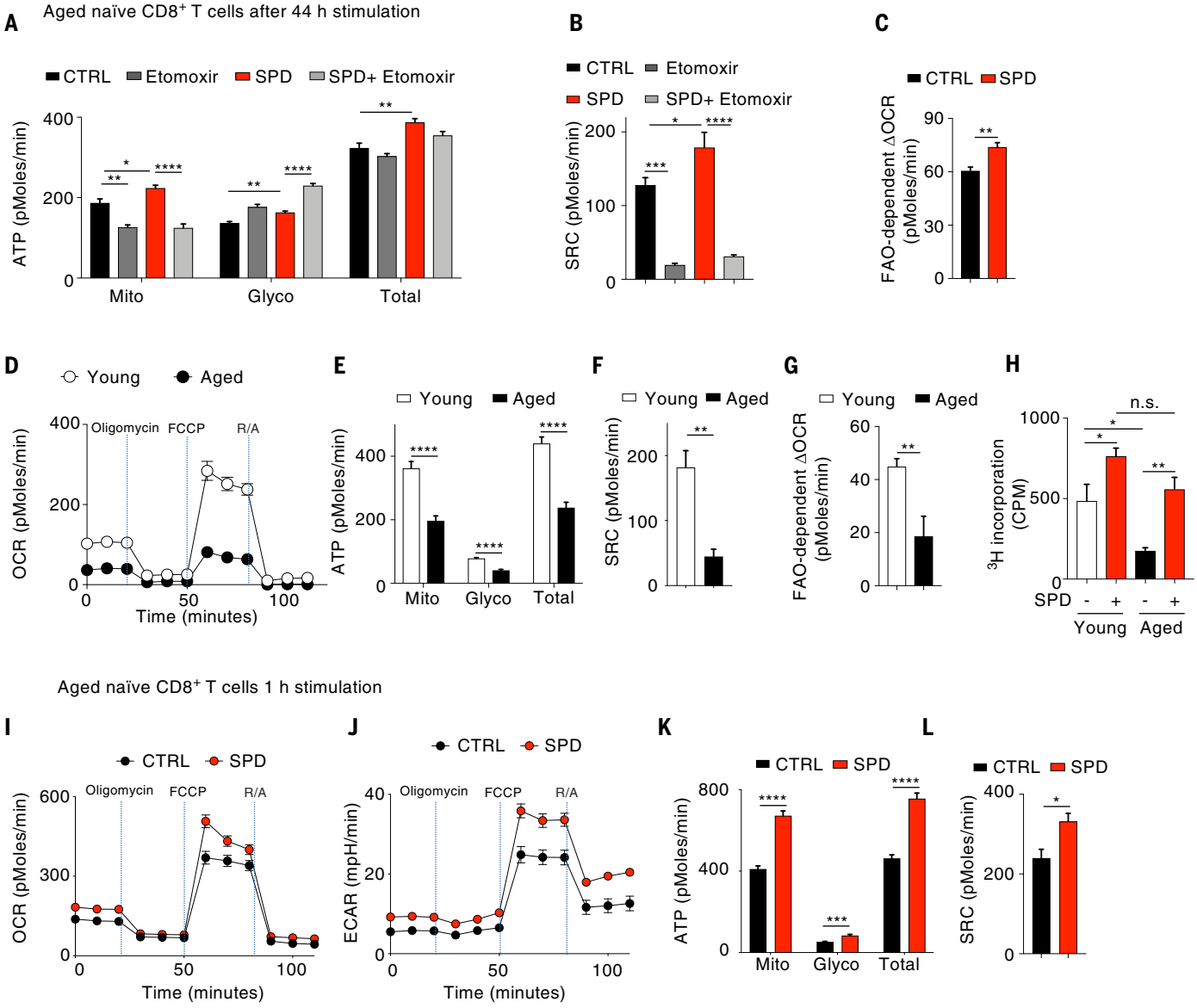

Fig. 2. SPD enhances mitochondrial respiration in a FAO-dependent manner. (**A** to **C**) Naïve CD8$^+$ T cells from aged mice were stimulated for 44 hours with anti-CD3 and anti-CD28 coated beads in the presence or absence of SPD. Etomoxir was added 1 hour before the assay. ATP production (A), SRC (B), and FAO-dependent OCR (C) were calculated as indicated in fig. S2, A to C (n = 4 technical replicates pooled from 12 mice). (**D** to **G**) Mitochondrial bioenergetics in naïve CD8$^+$ T cells isolated from young (white circle or bars) and aged mice (black circle or bars) (n = 4 to 5 technical replicates pooled from 4 young and 18 old mice). Real-time OCR (D), ATP production rate (E), SRC (F), and FAO-dependent coupled OCR (G) are shown. (**H**) Proliferation of naïve CD8$^+$ T cells from young and aged mice after 20 hours stimulation with anti-CD3 and anti-CD28 coated beads with and without SPD (n = 4 to 5 technical replicates). (**I** to **L**) Naïve CD8$^+$ T cells from aged mice were stimulated for 1 hour with anti-CD3 and anti-CD28 coated beads in the presence or absence of SPD (0.2 μM). OCR (I) and ECAR (J), ATP production rate (K), and SRC (L) are shown (n = 5 to 6 technical replicates). Data are the means ± SEMs [(D), (I), and (J)] or + SEMs [(A) to (C), (E) to (H), (K), and (L)]. P values were determined using unpaired two-tailed Student's t tests [(C), (E), (F), (G), (K), and (L)] or one-way ANOVA [(A), (B), and (H)]. *P < 0.05; **P < 0.01; ***P < 0.001; ****P < 0.0001; n.s, not significant. All data are representative of at least three independent experiments.

complex, responsible for β-oxidation of long-chain fatty acids (*27*, *28*). Western blotting experiments confirmed that the binding of HADHA and HADHB to SPD-coated FG beads was competitively decreased by the addition of 2 mM SPD to the mixing buffer (Fig. 3B). Similar binding of SPD to HADHA and HADHB was observed in mitochondrial lysates from Jurkat T cells (fig. S7A). We further confirmed the binding of SPD to HADHA and/or HADHB in situ by Duolink proximity ligation assay (PLA), in which the direct interactions between HADHA or HADHB proteins and SPD molecules were specifically detected as fluorescent spots by the interaction of two separate mAbs each to SPD or HADHA and HADHB (Fig. 3, C to E).

We expressed human HADHA and HADHB proteins in *E. coli* and purified the complex to homogeneity (Fig. 3, F and G). The purified protein complex with a single peak of 256 kDa in a gel filtration profile contained α and β subunits in an equal molar ratio, in agreement with the known $HADHA_2HADHB_2$ form (Fig. 3, H and I) (*27*, *28*). We confirmed that the antibody to SPD used in Duolink PLA recognized SPD bound to the purified $HADHA_2HADHB_2$ complex (fig. S7B). To test whether SPD binds to HADHA and HADHB independently, we also synthesized HADHA and HADHB separately in *E. coli*. Both HADHA and HADHB bound to

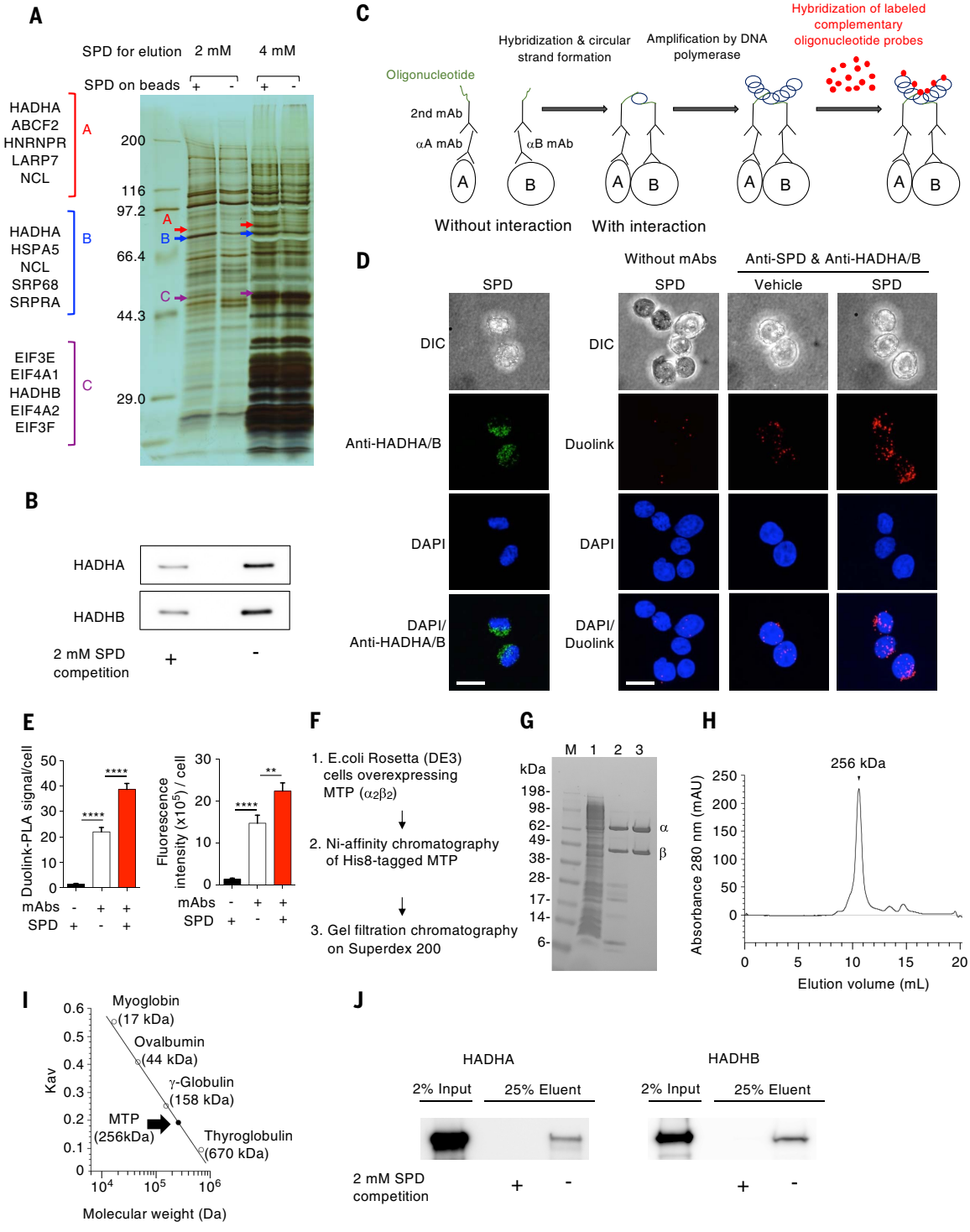

Fig. 3. SPD binds to HADHA and HADHB subunits of MTP. (**A**) Gel electrophoresis of HeLa cell lysate proteins captured by SPD-conjugated beads. Bands A, B, and C were eluted and subjected to mass spectrometry. The most abundant proteins in bands A, B, and C were listed on the left. (**B**) High concentration of SPD (2 mM) addition to HeLa cell lysate considerably decreased HADHA and HADHB proteins captured by SPD-conjugated beads. Bead-captured proteins were detected by HADHA- and HADHB-specific antibodies. (**C**) Illustrative figure of the principle of Duolink-PLA assay. (**D**) Molecular interaction between SPD and mitochondrial HADHA-HADHB (MTP) complex by in situ Duolink-PLA assay. Anti-SPD and anti-HADH antibodies were used for the assays. DIC, differential interference contrast; DAPI, 4′,6-diamidino-2-phenylindole. (**E**) The number and intensity of Duolink fluorescent dots (n = 19 to 25 cells). (**F**) Flow of human MTP purification steps. (**G**) Representative SDS-PAGE gel showing the purity of each step shown in (F). (**H**) Typical profile in gel filtration chromatography of the purified human MTP on a Superdex 200 Increase 10/300 GL column. mAU, milli–absorbance units (at the wavelength of 280 nm). (**I**) Calibration curve for the determination of the MTP molecular weight by gel filtration chromatography. (**J**) Separately produced HADHA and HADHB from *E. coli* were collected by SPD-conjugated beads. High dose of SPD addition to E. coli lysate decreased considerably, the HADHA or HADHB trapped by SPD-beads. Data are the means + SEMs (E). P values were determined using one-way ANOVA (E). $^{**}P < 0.01$; $^{****}P < 0.0001$. Data are representative of two to three independent experiments.

SPD beads, which was inhibited by the addition of free SPD (Fig. 3J).

SPD augments the PD-1 blockade efficacy by direct up-regulation of FAO enzymatic activity in T cells

During β-oxidation of long-chain fatty acids, the MTP complex catalyzes three out of four β-oxidation reactions—i.e., 2,3-enoyl-CoA hydrolase and 3-hydroxyl-CoA dehydrogenase (HAD) activities by HADHA and 3-ketothiolase (KT) activity by HADHB (Fig. 4A) (*27*–*29*). We thus examined the effect of SPD on the enzymatic kinetics of the purified $HADHA_2HADHB_2$ complex. SPD enhanced the HAD activity catalyzed by the HADHA subunit with a Michaelis constant (K_m) value of ~0.4 μM (Fig. 4B). SPD reduced the K_m value of NADH to the HAD enzyme and increased the maximum velocity of the enzymatic reaction (V_{max}). Thus, SPD may enhance the catalytic activity of HAD by allosteric binding to the HADHA subunit (Fig. 4C). SPD also activated the KT activity catalyzed by the HADHB subunit with a K_m value of ~0.7 μM (Fig. 4D). SPD also reduced the K_m value of acetoacetyl-CoA to the KT enzyme and appeared to shift the saturation curve of this substrate from the sigmoidal toward normal kinetics with apparently little change in V_{max}, supporting the allosteric effect of SPD on the MTP complex (Fig. 4E). We conclude that SPD interacts with both HADHA and HADHB subunits and allosterically activates their enzymatic activities.

To demonstrate physiochemical binding of SPD to the MTP complex in vitro, we used biolayer interferometry (BLI) (Octet). For this purpose, we expressed HADHA and HADHB separately in *E. coli*. We could purify $HADHA_2$ to homogeneity but failed to purify $HADHB_2$ as it showed heterogeneous peaks in a gel elution profile, suggestive of its hydrophobic properties (fig. S8). The biosensor tip, on the surface of which SPD was immobilized, was then immersed in a solution of purified $HADHA_2$ homodimer, and the difference in optical path length was traced in real time (Fig. 4F). Comparing two fitting model curves based on the binding molar ratio ($HADHA_2$:SPD = 1:1 or 1:2), we found that the 1:2 model, but not 1:1 model, fitted well, indicating that one purified $HADHA_2$ homodimer bound two SPD molecules with the binding affinity (dissociation constant, K_d) value of 0.10 μM. Because this method uses fixed SPD on the probe, the K_d value obtained tends to be much lower than the K_m value obtained by enzymatic kinetics (Fig. 4B).

Further depletion of CPT1a in a human T cell line (CPT1a knockdown Jurkat) abolished the acute enhancement effect of mitochondrial OCR by SPD (Fig. 4G and fig. S9A). To confirm that the SPD effect is mediated by MTP, we generated mice with specific deletion of HADHA in T cells (Fig. 4H). These mice showed frequencies of both $CD4^+$ and $CD8^+$ T cells, $CD44^{low}$ $CD8^+$ T cells, and $CD44^{high}$ $CD8^+$ T cells comparable to those in wild-type (WT) mice (fig. S9, B and C). The enhancement effects of SPD on OCR and tumor immunotherapy were not present in mice with T cell–specific deletion of HADHA (Fig. 4, I and J). Thus, we conclude that enhanced antitumor immunity by SPD supplementation depends in part on FAO activation through MTP, although we do not exclude other mechanisms.

Spermine competitively inhibits the FAO activity of SPD

FG beads coated with spermine, another natural polyamine derived from SPD, also bound to the $HADHA_2HADHB_2$ complex expressed in *E. coli* (fig. S10, A and B) and decreased SPD binding to the purified $HADHA_2HADHB_2$ complex (fig. S10B). Furthermore, spermine blocked SPD-induced activation of the HAD as well as KT activity of the purified MTP complex (fig. S10, C and D). Spermine decreased SPD-induced mitochondrial activation in a dose-dependent manner at both the early and late phases of $CD8^+$ T cell activation (fig. S10E). Additionally, norspermidine (norSPD), which does not have the moiety used for the hypusination reaction but shares the C_3-NH_2 structure with SPD and spermine, also increased mitochondrial ATP production in the later phase of activation (fig. S10, A and F). Within 20 hours, injected ^{13}C-labeled SPD was not metabolized into spermine, indicating that most injected SPD works directly as a positive regulator of FAO activity (fig. S11, A and B). Thus, it is likely that the late-phase mitochondrial activation by SPD may also be primarily a consequence of the activation of MTP.

Discussion

We showed that SPD acutely increased FAO and ATP production by direct activation of MTP in $CD8^+$ T cells, subsequently leading to de novo synthesis of proteins related to OXPHOS and translation. SPD binding and the activation of MTP may initiate a series of events, ultimately leading to enhanced mitochondrial metabolism. Hypusination of eIF5A may have critical roles in protein synthesis in a later phase of the SPD effect, although the relative contribution of these two mechanisms remains to be clarified. The K_m value (6.49 μM) of SPD to deoxyhypusine synthase is 10 times as high as that for MTP (0.4 to 0.7 μM in Fig. 4) (*30*). The inhibition of EP300 protein acetylase activity was demonstrated in vitro using 10 μM SPD, 50 times that required for MTP activation (*31*). These results support the possibility that MTP activation is the earliest and most efficient function of SPD. The current molecular mechanistic analysis of SPD function in $CD8^+$ T cells provides insight into the antiaging properties of SPD and may facilitate a better understanding of the strategies to prevent age-related immune diseases. SPD and caloric restriction mimetics induce drastic changes in the metabolome, resulting in autophagy. Also, starvation induces autophagy and promotes longevity, whereas exogenous lipid exposure inhibits autophagy (*32*, *33*). Although lipid metabolism is closely linked to autophagy, its precise mechanism is still unknown (*34*). SPD administration has effects similar to those of starvation, preventing damage from exogenous lipid exposure and inducing autophagy within a few hours after administration (*31*, *35*, *36*). SPD is likely to induce a metabolic shift through FAO activation by allosteric binding to the MTP complex. Because the MTP complex also functions in energy production through FAO in other tissues, such as skeletal muscles and the heart, liver, and brain, in addition to the immune cells (*19*, *37*–*39*), the current mechanism of FAO activation by SPD might be applicable to a whole-body antiaging effect of SPD. Although the FAO up-regulation by SPD demonstrated in this work may not represent its sole mechanism for longevity, it may be one of the critical pathways to maintain normal functions of various organs.

Materials and methods

Mice

Young C57BL/6N or BALB/c (1 to 3 months old) and aged C57BL/6N (>1 year old) mice were purchased from Charles River Laboratories Japan. C56BL/6N-background $HADHA^{flox}$ mice were purchased from Cyagen Biosciences. CD4 Cre were maintained at the Institute of Laboratory Animals, Graduate School of Medicine, Kyoto University (*40*). All mice were used under protocols approved by the respective institutional review board (IRB). All mice were maintained under specific pathogen–free (SPF) conditions.

Cell lines

Details of murine colon adenocarcinoma (MC38), Lewis lung carcinoma (LLC), and colon carcinoma (CT26) cell lines were described previously (*41*). MC38, CT26, and Jurkat cell lines were cultured in RPMI medium (Gibco) with 10% (v/v) heat-inactivated fetal calf serum (FCS) and 1% (v/v) penicillin–streptomycin mixed solution (Nacalai tesque). HeLa and LLC cells were cultured in DMEM medium (Gibco) with 10% (v/v) heat-inactivated fetal calf serum (FCS) and 1% (v/v) penicillin–streptomycin mixed solution (Nacalai tesque).

Chemical reagents

The following chemical reagents were used at the indicated concentrations for the combination therapy, mitochondrial activity assays, and MTP functional assays. SPD (Nacalai tesque) prepared in MiliQ as solvent (CTRL),

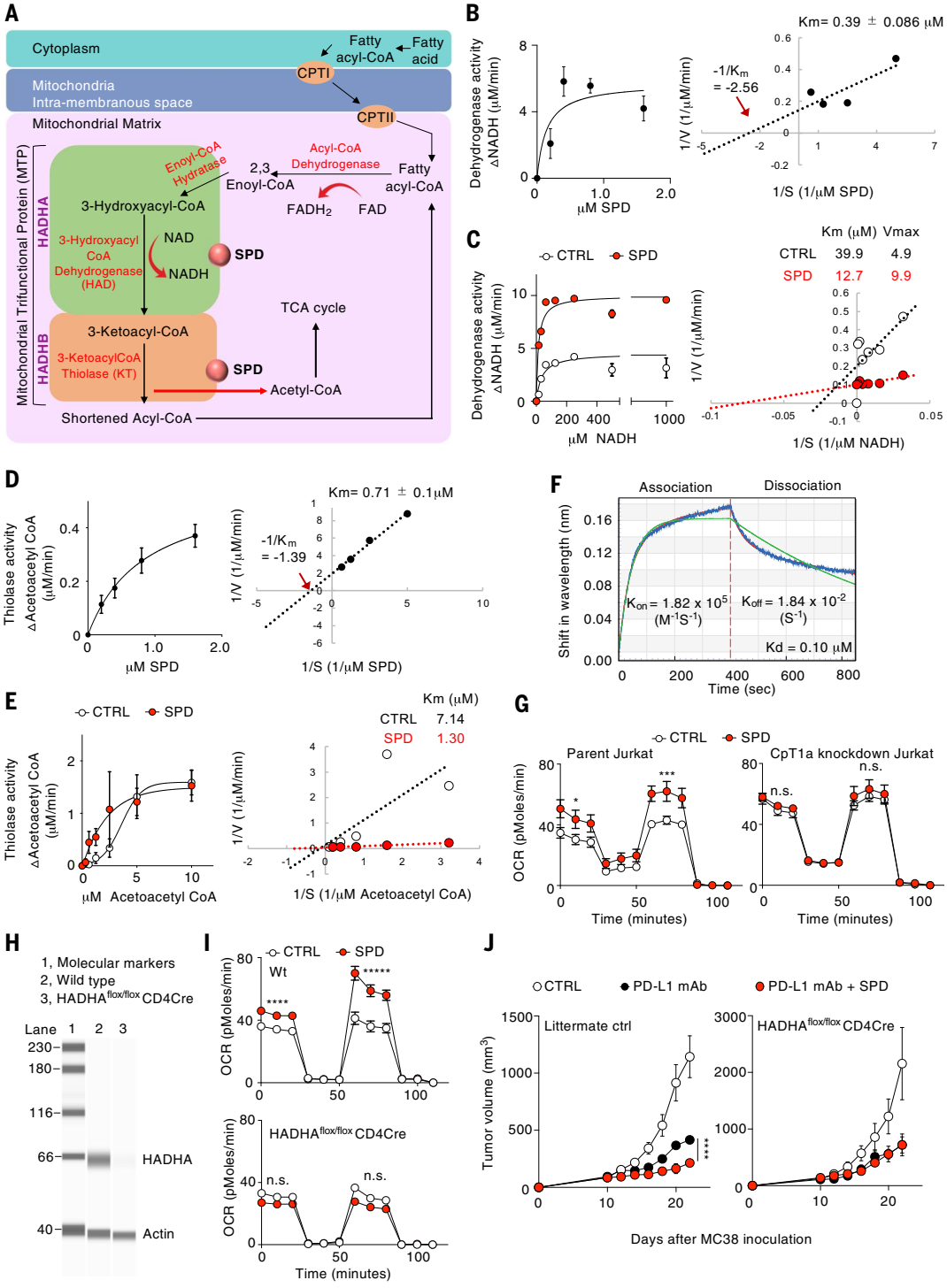

Fig. 4. SPD allosterically activates enzymatic activities of MTP. (**A**) A schematic diagram of the MTP complex and the enzymatic activities mediated by the HADHA and HADHB subunits. Long-chain fatty acids are transported into the mitochondria by carnitine and fatty acyl-CoA is catabolized by three steps of β-oxidation activity of MTP. (**B**) The effect of different doses of SPD on the dehydrogenase activity of the HADHA subunit in purified human MTP. The enzymatic activity was evaluated by the reduction of NADH in reverse reaction (left) (n = 4 technical replicates; HAD activity without SPD is used as a baseline to adjust the measurements in this graph). The best fit line of (1/V versus 1/SPD concentration) gave the K_m (K_d) value (right). (**C**) The effect of SPD on the NADH affinity in dehydrogenase activity of HADHA (left) (n = 5 technical replicates). The best fit line of (1/V versus 1/NADH concentration) gave the K_m and V_{max} value. (**D**) The effect of different doses of SPD on the 3-ketoacyl thiolase activity of HADHB subunit in purified human MTP. The enzymatic activity was evaluated by the reduction of acetoacetyl CoA in forward reaction (left) (n = 6 technical replicates; KT activity without SPD is used as a baseline to adjust the measurements in this graph). The best fit line of (1/V versus 1/SPD concentration) gave the K_m (K_d) value (right). (**E**) The effect of SPD on the acetoacetyl CoA affinity to HADHB in MTP (left) (n = 5 technical replicates). The best fit line of (1/V versus 1/ acetoacetyl CoA concentration) gave the K_m value (right). (**F**) Octet analysis of the molecular binding between SPD and the $HADHA_2$ homodimer. Green and red smooth lines represent models fitted by 1:1 and 1:2 binding stoichiometry, respectively. Actual binding data (blue wavy line) fit well to the 1:2 bivalent model, indicating that the $HADHA_2$ homodimer binds two SPD on the surface of the Octet probe. (**G**) CPT1a was knocked down by CRISPR interference system on human T cell line, Jurkat. In the medium with low glucose and high palmitate, the effect of SPD on the OCR of parent and CPT1a-knockdown Jurkat were evaluated (n = 3 to 5 technical replicates, unpaired two-tailed Student's t tests of the second point in each step of OCR assay). (**H**) Western blotting assay of protein levels of HADHA in $CD3^+$ T cells of T cell–specific HADHA knockout mice ($HADHA^{flox/flox}$ CD4Cre mice). (**I**) OCR of naïve $CD8^+$ T cells from $HADHA^{flox/flox}$ CD4 Cre or WT mice stimulated with anti-CD3 and anti-CD28 coated beads with or without SPD for 1 hour in the medium with low glucose and high palmitate (n = 6 technical replicates). (**J**) The effect of SPD combination on the MC38 growth in littermate control (ctrl) or $HADHA^{flox/flox}$ CD4Cre mice [n = 3 mice (PD-L1 mAb or PD-L1 mAb + SPD for control mice), 4 mice (PD-L1 mAb or PD-L1 mAb + SPD for $HADHA^{flox/flox}$ CD4Cre mice), or 5 mice (the other groups), with male and female mice distributed equally among the groups]. Data are the means ± SEMs [(B) to (E), (G), (I), and (J)]. P values were determined using multiple unpaired Student's t tests [(G) and (I) in the second point after each step of OCR assay] or two-way ANOVA [(J) on day 22]. $^{**}P < 0.01$; $^{***}P < 0.001$; $^{****}P < 0.0001$; n.s, not significant. Data are representative of two or more independent experiments.

spermine (Nacalai tesque), norSPD (Sigma-Aldrich), GC7 (EMD Milipore), etomoxir (Sigma-Aldrich), acetoacetylCoA (Cayman chemical company), NADH (Nacalai tesque), CoA (Sigma-Aldrich), and ^{3}H thymidine (PerkinElmer). Other chemical reagents used were equipped with the kits.

Mouse therapy model

MC38 (5×10^5), LLC (2×10^6), or CT26 (1×10^6) were intradermally (i.d.) injected on the right flank (day 0) into C57BL/6N or BALB/c mice. For treatment, the mice were intraperitoneally (i.p.) injected with 40 μg of anti–PD-L1 mAb (clone 1-111A, made in house) alone (*42*) or in combination with SPD 9 to 10 days after tumor inoculation. Anti–PD-L1 mAb and SPD were injected every 5 days until day 30. Tumor measurement was performed on each alternate day, and tumor volume was calculated using the formula for a typical ellipsoid: 3.14 × (length × breadth × height) / 6.

In vivo analysis

For in vivo analysis, MC38 tumor–bearing mice were treated with PD-L1mAb and SPD 10 days after tumor injection and euthanized on day 13. Cells from the DLNs [axillary, brachial, and inguinal lymph nodes (LNs)] on the right side of tumor-bearing mice were harvested. All LNs were homogenized and pooled. For TIL analysis, tumor samples were minced into 1- to 2-mm pieces with scissors and digested with collagenase type IV (Thermo Fisher Scientific) using a gentleMACS Dissociator (Miltenyi Biotec). The number of TILs per milligram was used to calculate absolute numbers. For peripheral blood mononuclear cells (PBMCs) analysis, 100 μl of blood was collected and then treated with ammonium-chloride-potassium lysing buffer to lyse red blood cells. To check the mitochondrial activity, total CD8$^+$ T cells were sorted from pooled DLNs using autoMACS Pro Separator (Miltenyi Biotec, 130-1117-004) and used for Seahorse. The total CD8$^+$ T cells were also stimulated with anti-CD3 and -CD28 mAb beads (Thermo Fisher Scientific) for 20 hours and used to measure the proliferation by thymidine incorporation assay (*41*). The supernatant after the stimulation was used to measure IFN-γ secretion by enzyme-linked immunosorbent assay (ELISA) (Biolegend, 430804) according to the manufacturer's instructions.

Absolute quantification of polyamines by liquid chromatography–mass spectrometry (LC-MS)

Sample preparation

For polyamine quantification in the serum of mice, whole blood was collected from the cranial vena cava and allowed to clot undisturbed at room temperature for 1 hour. The clot was then removed by sequential refrigerated centrifugation at 14,500 rpm for 15 min. Serum was collected to new tubes and then centrifuged for another 8 min. Serum was aliquoted and used for analysis.

For polyamine quantification in naïve CD8$^+$ T cells, pooled peripheral LN (pLN) and spleen cells were used for sorting naïve CD8$^+$ T cells by Mojosort system (BioLegend MojoSort: 480035). The cells were stained using CD8 (53-6.7) and CD44 (1M7) antibodies, and CD44$^-$ cells (naïve fraction) were sorted using BD FACSAria (BD Biosciences). For total SPD concentrations, 1×10^6 cells pellets were used for analysis. To measure free SPD concentrations, cells were homogenized in 150 μl of RNase-free, DNase-free, and protease-free water (Nacalai tesque) for 5 min on ice using Violamo Homogenizer Pestle. Then 150 μl of 70% alcohol was added, and RNAs were removed using RNA binding columns (Qiagen, 74104). The samples were subsequently filtered using DNA binding columns (Qiagen, 27106) to removed DNA and using Ultrafree-MC-PLHCC centrifugal filters (Milipore, UFC3LCCNB-HMT) to remove proteins. Filtered samples were used for analysis.

Quantification

Polyamine concentration in blood cells and serum was quantified by the internal standard method. To the filtered solution was added 200 μl of methanol containing isotopically labeled polyamines [0.01 μM, spermidine-(butyl-$^{13}C_4$) trihydrochloride, spermine-(butyl-d8) tetrahydrochloride, putrescine-15N2 dihydrochloride]. After centrifugation at 16,000 ×*g* for 30 min at 4°C, 250 μl of the supernatant was collected and dried using vacuum centrifugation. The dried sample was resuspended in 20 μl of 0.1% formic acid in water and then subjected to LC-MS analysis. Authentic standards of SPD (spermidine trihydrochloride) and spermine (spermine tetrahydrochloride) were purchased from SIGMA Aldrich. Putrescine was purchased from Tokyo Chemical Industry. Standard solutions were prepared at the concentration of 0.0002, 0.0004, 0.001, 0.002, 0.005, 0.01, 0.02, 0.05, and 0.1 and treated with the same procedure as the sample. The cellular concentration of polyamines was calculated, taking into account the mean cell volumes of each group (young = 302 fl; aged = 443 fl) estimated from measured cell diameter. The cell volume was significantly different between young and aged mouse ($P < 0.001$, Wilcoxon rank sum test). For serum samples, the protocol was slightly changed. Briefly, 50 μl of serum was treated with 250 μl of methanol for polyamine extraction, and the standard curve range was 0.01 to 4 μM. The correlation coefficient of standard curve was higher than 0.99. LC separation was conducted on a Shim-pack GIST C18-AQ column (3 μm, 150 mm × 2.1 mm id, Shimadzu GLC) with a Nexera UHPLC system (Shimadzu). The mobile phase consisted of 0.1% formic acid in water (A) and 0.1% formic acid in acetonitrile (B). The gradient program was as follows: 0 to 3 min, 0% B; 3 to 15 min, linear gradient to 60% B; 15 to 17.5 min, 95% B; 17.5 to 20.0 min, linear gradient to 0% B; hold for 4 min; flow rate, 0.2 ml/min. The column oven temperature was maintained at 40°C. The LC system was coupled with a triple-quadruple mass spectrometer LCMS-8060 (Shimadzu). LCMS-8060 was operated with the electrospray ionization and multiple reaction monitoring mode. The ion transitions (precursor–product ion) for SPD, spermidine $^{13}C_4$, spermine, spermine d8, putrescine, and putrescine 15N2 were *m*/*z* (mass/charge ratio) 146.2 to 72.1, 150.2 to 76.1, 203.2 to 112.1, 211.3 to 120.1, 89.1 to 72.1, and 91.1 to 73.0, respectively.

Cell preparation for in vitro analysis

For in vitro mitochondrial activity assays, cells from axillary, brachial, and inguinal pLNs on both sides of mice without tumor were harvested, homogenized, and pooled. Spleens were harvested and homogenized and then treated with ammonium-chloride-potassium (ACK) lysing buffer for 2 min to lyse red blood cells. After pooling the cells of pLNs and spleens, naïve (CD44^{low}) CD8$^+$ T cells were purified using MojoSort system (BioLegend MojoSort: 480044) according to the manufacturer's instructions and used for Seahorse assays. For effector memory (CD44^{high}) CD8$^+$ T cells in vitro experiments, total CD8$^+$ T cell were first sorted from pooled LN and spleen cells using CD8$^+$ T cell Mojosort system (BioLegend MojoSort: 480035). The cells were then stained using CD8 (53-6.7) and CD44 (1M7) antibodies, and CD44$^+$ cells (effector memory fraction) were sorted using BD FACSAria (BD Biosciences). For Jurkat experiments, 24 hours before the seahorse assay, the cells were transfered to low-glucose (2.5 mM) RPMI medium.

Mitochondrial activity and ATP production rate measured by Seahorse

Isolated cells were seeded in an XFe96 plate (3 to 5×10^5 and 8×10^4 cells per well for the assays of primary cells and cell line, respectively), and their OCR and ECAR were measured by the XFe96 Extracellular Flux Analyzer (Seahorse Bioscience) as previously described (*21*). The three pharmaceutical modulators of mitochondrial OXPHOS, which were included in the XF Cell Mito Stress Test Kit (Seahorse Bioscience), were used for OCR and ECAR measurement (*22*). For these assays, XF DMEM Base Medium (Agilent, 103575-100) was used, supplemented with 1 mM HEPES (pH 7.4), 1 mM pyruvate (Nacalai Tesque), 2 mM glutamine (Nacalai Tesque), and 10 mM glucose (Nacalai Tesque). For the FAO measurement in CD8$^+$ T cells isolated from in vivo treated mice, XF RPMI Base Medium (Agilent, 103576-100) was used, supplemented with 1 mM HEPES

(pH 7.4), 2.5 mM glucose, and 0.75 mM carnitine (Sigma-Aldrich) on the day of the assay. Oligomycin (1.5 μM), carbonyl cyanide 4-(trifluoromethoxy) phenylhydrazone (FCCP) (1 μM), and rotenone/antimycin A (1 μM) were injected sequentially. Each parameter of mitochondrial activity was defined as follows (details in fig. S2, A and B). Basal OCR was defined as (the last rate measurement before oligomycin injection) – (nonmitochondrial respiration rate after rotenone/antimycin injection). Maximal OCR was defined as (the first rate-measurement after FCCP injection) – (nonmitochondrial respiration rate). OCR coupled with ATP production (coupled OCR) was defined as (basal OCR) – (the last rate-measurement before FCCP injection). OCR uncoupled with ATP production (uncoupled OCR or SRC) was defined as (maximal OCR) – (basal OCR). Mitochondrial and glycolytic ATP production rates were automatically calculated by the Seahorse machine operating software (Wave) based on the coupled OCR and the ECAR, the difference between measurements before and after oligomycin injection, respectively. FAO-dependent OCR (ΔOCR) was defined as the (OCR untreated with etomoxir) – (OCR treated with etomoxir) (details in fig. S2C). Etomoxir (5 μM) or dimethyl sulfoxide (DMSO) (as solvent control) were added 50 min before running the assay. Palmitate (100 to 200 μM) or bovine serum albumin (BSA) (as solvent control) were added to the correspondent groups 30 s before running the assay.

Mitochondrial activity in response to SPD and etomoxir in situ injection measured by Seahorse

Isolated cells (8×10^4 per well) were seeded in an XFe96 plate coated or uncoated with functional grade CD3/CD28 mAb. OCR was then measured by the XFe96 Extracellular Flux Analyzer (Seahorse Bioscience). The measurement protocol was modified so that the machine injects SPD (final concentration of 0.2 μM) from the first port and etomoxir (final concentration of 3 μM) from the second port. Oligomycin (final concentration of 1.5 μM) was injected from the thirst port and rotenone/antimycin A (final concentration of 1 μM) from the fourth port. For these assays, XF RPMI Base Medium (Agilent, 103576-100) was used, supplemented with 1 mM HEPES (pH 7.4), 2.5 mM glucose, 0.75 mM carnitine (Sigma-Aldrich) and 200 μM palmitate (Cayman) on the day of the assay

Proteomics

Preparation of unlabeled tryptic peptide samples for data-independent acquisition mass spectrometry (DIA-MS)

Tryptic peptide samples were prepared following the phase transfer surfactant method (*22*), with modifications described as follows: Protein extracts were prepared from 4×10^5 cells in 10 μl of lysis buffer containing 12 mM sodium deoxycholate, 12 mM sodium N-dodecanoylsarcosinate, and 100 mM Tris-HCl pH 9.0, with complete EDTA-free protease inhibitor cocktail (Roche). To reduce and alkylate the disulphide bonds, DL-dithiothreitol was added to 10 mM with incubation at 50°C for 30 min, followed by iodoacetamide added to 40 mM at room temperature for 30 min the dark, then cysteine was added to 55 mM for 10 min to quench the alkylation reactions. Samples were diluted 1:2.76 with 50 mM ammonium bicarbonate solution. Mass spectrometry–grade lysyl endopeptidase (FUJIFILM Wako Chemical Corporation) was added at 200 ng, after mixing, 200 ng sequencing grade modified trypsin (Promega) was added, followed by protein digestion at 37°C for 14 hours. Afterward, 1.83 volumes ethyl acetate was added together with trifluoroacetic acid (TFA) to 0.5% (v/v). Centrifugation at 12,000 ×*g* for 5 min produced an upper organic phase which was discarded and a lower aqueous phase containing digested tryptic peptides, which was dried using a centrifugal vacuum concentrator. Afterward, samples were desalted with ZipTip C18, 0.6 μl Pipette Tips (MilliporeSigma) and dried.

The protein concentration of protein extracts in lysis buffer was determined using a Pierce BCA Protein Assay Kit (ThermoFisher Scientific). From each sample, 5 μg protein at a concentration of 0.5 μg/μl was used to prepare digested tryptic peptide samples, as described above. Afterward, the tryptic peptide samples were desalted with MonoSpin C18 columns (GL Sciences Inc.) and dried using a vacuum centrifuge. To generate a spectral library, a combined sample containing tryptic peptides from each sample condition was fractionated using a Pierce High pH Reversed-Phase (HPRP) Fractionation Kit, according to the manufacturer's instructions (ThermoFisher Scientific).

Mass spectrometry measurement for proteomic analysis

For liquid chromatography with tandem mass spectrometry (LC-MS/MS), a Q-Exactive Plus Orbitrap mass spectrometer with an attached Nanospray Flex ion source connected to an EASY-nLC 1200 system was used (ThermoFisher Scientific). The peptides were separated using an analytical column with 3 μm C18 particles, an inner diameter of 75 μm and a length of 12.5 cm (Nikkyo Technos Co., Ltd.). Solvents were LC/MS grade. LC solvent A consisted of 0.1% (v/v) formic acid in water and LC solvent B consisted of 0.1% (v/v) formic acid in 80% (v/v) acetonitrile. The flow rate was 300 nl/min with a 2-hour gradient: 0 to 108 min (2% B to 34% B), 108 to 110 min (34% B to 95% B), and 110 to 120 min consisted of a final wash at 95% B. A 2.0-kV spray voltage was applied, and the ion transfer tube temperature was 250°C.

For data-dependent acquisition (DDA) measurement of the TMT-labeled peptide samples, the peptides were dissolved in 6.8 μl of 0.1% (v/v) formic acid, 3% (v/v) acetonitrile in water, and 5 μl was measured. The full MS spectra were acquired from 380 to 1400 m/z at a resolution of 70,000, the automatic gain control (AGC) target was 3×10^6, with a maximum injection time (IT) of 50 ms. MS^2 scans were recorded for the top 15 precursors at 17,500 resolution with an AGC target of 2×10^5 and a maximum IT of 100 ms. The isolation window was set at 0.7 m/z with a fixed first mass of 105.0 m/z. The default charge state was 2. HCD fragmentation was set to normalized collision energy of 32%. The intensity threshold was 8.0×10^3, charge states 2 to 5 were included, and the dynamic exclusion was set to 20 s.

For data-independent acquisition (DIA), the peptide samples were dissolved in 10 μl of 0.1% (v/v) formic acid, 3% (v/v) acetonitrile in water, and 3 μl was loaded. Data were acquired with 1 full MS and 32 overlapping isolation windows constructed covering the precursor mass range of 400 to 1200 m/z. For full MS, resolution was set to 70,000, AGC target was 5×10^6, and the IT was 120 ms. DIA segments were acquired at 35,000 resolution with an AGC target of 3×10^6 and an automatic maximum IT. The first mass was fixed at 200 m/z. HCD fragmentation was set to normalized collision energy of 27%.

For data-dependent acquisition (DDA) of unlabeled HPRP-fractionated peptide samples, each fraction was dissolved in 6.5 μl of 0.1% (v/v) formic acid, 3% (v/v) acetonitrile in water, and 5.0 μl was loaded. The full MS spectra were acquired from 380 to 1500 m/z at a resolution of 70,000, the AGC target was 3×10^6 and a maximum IT of 100 ms. The MS^2 scans were recorded for the top 20 precursors at 17,500 resolution with an AGC target of 1×10^5 and a maximum IT of 60 ms. The isolation window was 2.2 m/z. The default charge state was 2. HCD fragmentation was set to normalized collision energy of 27%. The intensity threshold was set to 1.3×10^4, charge states 2 to 5 were included, and the dynamic exclusion was set to 20 s.

Protein identification and quantification in proteomic analysis

For analysis of the DIA data, a spectral library was first generated from the eight raw data files obtained from DDA measurement of the HPRP-fractionated unlabeled samples using Proteome Discoverer version 2.4 with the Uniprot reviewed *Mus musculus* (taxon 10090) database. The filtered output from Proteome Discoverer was used to generate a sample-specific spectral library using Spectronaut software (Biognosys). Raw data files from DIA measurement were used for extraction of peptide quantities with the generated spectral

library and integration of these quantities into protein abundances. False discovery rate (FDR) was estimated with the mProphet approach and set to 0.01 at both peptide precursor level and protein level (*43*, *44*). Data filtering parameters for quantification were Q-value percentile fraction 0.5 with global imputing, and cross run normalization with global normalization on the median.

In vitro metabolic trace analysis of ^{13}C-labeled palmitate and SPD

For palmitate-$^{13}C_{16}$ tracing, naïve CD8$^+$ T cells were sorted from LNs and spleens of 3-month-old mice and cultured in glutamine/glucose/FBS-free RPMI-1640 medium (Wako) supplemented with 1× MEM NEAA, 10 mM HEPES, 50 μM 2-mercaptoethanol, 100 U/ml penicillin, 100 U/ml streptomycin, 500 μM L-carnitine hydrochloride (Sigma), and 200 μM BSA-conjugated palmitate-$^{13}C_{16}$ (Isotec). Cells were stimulated for 1 hour in the presence of anti-CD3 and -CD28 mAb beads (Thermo Fisher Scientific) with and without 0.2 μM SPD (Nacalai).

For SPD-(butyl-$^{13}C_4$) tracing, naïve CD8$^+$ T cells were cultured in RPMI-1640 medium (Wako) with glutamine/glucose supplemented with 10% (v/v) dialyzed FBS (Thermo Fisher Scientific), 1× MEM NEAA, 10 mM HEPES, 50 μM 2-mercaptoethanol, 100 U/ml penicillin, 100 U/ml streptomycin, and 1 mM sodium pyruvate. Cells were stimulated as described above for 1 and 20 hours with and without 0.2 μM spermidine-(butyl-$^{13}C_4$) (Sigma).

Metabolite extraction from cultured cells for metabolome analyses was performed as described previously (*45*). Briefly, cells were washed twice with cold phosphate-buffered saline (PBS), and residual wash solvent was carefully removed. Cells were then immediately frozen into liquid nitrogen and stored at −80°C until assayed. The frozen cultured cells were scraped with methanol containing internal standards (450 μl) followed by the addition of 500 μl of chloroform and 250 μl of ultrapure water. After centrifugation, the aqueous phase was ultrafiltered using an ultrafiltration tube (Ultrafree MC-PLHCC; Human Metabolome Technologies, Inc., Yamagata, Japan). Then, the filtrate was concentrated with a vacuum concentrator. The concentrated filtrate was dissolved in 50 μl of ultrapure water and used for LC-MS/MS and IC-MS analyses.

Mass spectrometry analysis to detect ^{13}C-labeled metabolites

For metabolome analysis focused on glycolytic metabolites, TCA cycle intermediates as well as ketone bodies, anionic metabolites were measured using an orbitrap-type MS (Q-Exactive focus; Thermo Fisher Scientific) connected to a high-performance ion chromatography (IC) system (ICS-5000+, Thermo Fisher Scientific) that enabled us to perform highly selective and sensitive metabolite quantifications owing to the IC-separation and Fourier Transfer MS principle. The IC was equipped with an anion electrolytic suppressor (Thermo Scientific Dionex AERS 500) to convert the potassium hydroxide gradient into pure water before the sample entered the mass spectrometer. The separation was performed using a Thermo Scientific Dionex IonPac AS11-HC, 4-μm particle size column. The IC flow rate was 0.25 ml/min supplemented post-column with 0.18 ml/min makeup flow of MeOH. The potassium hydroxide gradient conditions for IC separation were as follows: from 1 mM to 100 mM (0 to 40 min), 100 mM (40 to 50 min), and 1 mM (50.1 to 60 min), at a column temperature of 30°C. The Q Exactive focus mass spectrometer was operated under an ESI negative mode for all detections. Full mass scan (m/z 70 to 900) was performed at a resolution of 70,000. The automatic gain control target was set at 3×10^6 ions, and the maximum ion injection time was 100 ms. Source ionization parameters were optimized with the spray voltage at 3 kV, and other parameters were as follows: transfer temperature = 320°C, S-Lens level = 50, heater temperature = 300°C, Sheath gas = 36, and Aux gas = 10. The amount of cat ionic metabolites including amino acids were quantified using LC-MS/MS (*45*). Briefly, a triple-quadrupole mass spectrometer equipped with an electrospray ionization (ESI) ion source (LCMS-8060, Shimadzu Corporation) was used in the positive and negative-ESI and multiple reaction monitoring (MRM) modes. The samples were resolved on the Discovery HS F5-3 column (2.1 mmI.D. x 150 mmL, 3 μm particle, Sigma), using a step gradient with mobile phase A (0.1% formate) and mobile phase B (0.1% acetonitrile) at ratios of 100:0 (0 to 5 min), 75:25 (5 to 11 min), 65:35 (11 to 15 min), 5:95 (15 to 20 min), and 100:0 (20 to 25 min), at a flow rate of 0.25 ml/min and a column temperature of 40°C.

Preparation of SPD FG beads

Immorbilization of SPD on NHS FG magnetic beads (TAS8848 N1141, Tamagawa Seiki) was carried out according to the manufacturer's instruction. Briefly, 2.5 mg of NHS beads, which have a binding capacity for ~600 nmol of SPD, were washed twice with DMF (N,N-dimethylformamide, Nacalai Tesque) and then mixed with 5 mM SPD (Nacalai Tesque) dissolved in DMF. After dispersion by sonication, beads were incubated for 70 min at room temperature on a micro tube mixer. Then, beads were centrifuged at 15,000 rpm for 5 min to remove supernatant. 500 μl of 1M aminoethanol (Nacalai Tesque) in DMF was added to the beads, followed by dispersion by sonication. Beads were incubated further for 1 hour at room temperature. After being washed three times by 50% methanol, beads were stored in 150 μl of 50% methanol at 4°C.

Affinity purification with SPD FG beads

Cytoplasmic lysates of HeLa cells were dialyzed against KCl binding buffer [20 mM Hepes (pH 7.9), 100 mM KCl, 1 mM $MgCl_2$, 0.2 mM $CaCl_2$, 0.2 mM EDTA, 0.1 mM DTT, 0.1% NP-40, 10% (v/v) glycerol, supplemented with 1x protease inhibitor cocktail (Nacalai Tesque)]. For affinity purification, 50 μl of SPD FG beads were washed three times with the KCl binding buffer by sonication and centrifugation and then mixed with 500 μl of cell cytoplasmic lysates (~2 mg/ml of protein). As a negative control, SPD was added to the lysate to 2 mM for 1 hour competition at 4°C before mixing with the SPD beads. After being incubated for 4 hours at 4°C on a rotator, SPD beads were isolated by magnetic separation, and then suspended in the KCl binding buffer by sonication. Magnetic separation and sonication were repeated twice. After the final wash, elution buffers [20 mM Hepes (pH 7.9), 100 mM NaCl, 1 mM MgCl2, 0.2 mM CaCl2, 0.2 mM EDTA, 0.1 mM DTT, 0.1% NP-40, 10% (v/v) glycerol] containing 2 and 4 mM of SPD were mixed thoroughly with the beads by sonication, followed by 1 hour incubation at 4°C on a micro tube mixer for elution. Beads were separated magnetically, and eluates were subjected to SDS–polyacrylamide gel electrophoresis (SDS-PAGE). Gels were stained by EzStain Silver (ATTO), and protein bands were excised for mass spectrometric analysis. Affinity purification with spermine FG beads were conducted in the same way.

For the affinity purification from the lysate of Jurkat mitochondria, mitochondria were isolated using the EzSubcell Farction kit (WSE-7422, ATTO) according to the manufacturer instructions. They were then lysed in 2 volumes of lysis buffer [10 mM HEPES-NaOH (pH 7.9), 10 mM KCl, 1% NP40, 0.1 mM EDTA, 1 mM DTT, 0.5 mM PMSF] and then centrifuged at 13,500 ×g for 2 min. The supernatants were collected and diluted 10 times with pull-down buffer [820 mM HEPES (pH7.9), 100 mM KCl, 0.1% NP-40, 1 mM $MgCl_2$, 0.2 mM $CaCl_2$, 0.2 mM EDTA, 10% (v/v) glycerol, 1 mM DTT, 0.2 mM PMSF]. Affinity purification using SPD-immorbilized beads was performed as described above.

Western blotting

For HADHA and HADHB detection in the FG bead experiments, pull-downed samples were subjected to SDS-PAGE and transferred to TransBlot Turbo PVDF membranes (Bio-Rad). The following antibodies were used for detection: HADHA and HADHB (1/300, HPA015536, HPA066099, Atlas Antibodies, respectively) and rabbit immunoglobulin G (IgG) HRP (1/20000, no. 7074, Cell Signaling Technology).

Membrane was blocked with 5% (w/v) nonfat dry milk (Nacalai Tesque) for 1 hour at room temperature and then incubated with primary antibodies at 4°C overnight. The following day, secondary antibodies conjugated to horseradish peroxidase (HRP) were incubated for 1 hour at room temperature. Proteins were detected by Chemi-lumi One Ultra ECL Western Blotting Substrate (WAKO).

For the detection of HADHA protein from the T cells of $HADHA^{flox/flox}$ CD4 Cre mice and CPT1a knockdown Jurkat, T cell lysates were run through the automated Simple Western system, Jess according to the instructions (ProteinSimple Japan K.K.). The following antibody was used for detection; HADHA (1/100, 60250-1-Ig, Proteintech), CPT1a (1/250, ab128568, abcam) and beta-actin (1/250, no. 1978, Sigma), anti-Mouse Detection Module (MD-002A, biotechne). Mitochondrial morphology- and autophagy-related proteins Mitofusin (1/250, no. 9482, CST), Atg5 (1/250, no. 12994, CST), and Atg7 (1/50, no. 8558, CST) in stimulated T cells were detected in the similar way.

BLI experiment

Measurement of binding kinetics was performed by the BLI method using the Octet K2 system (Fortebio), according to the manufacturer's protocols. 10 mM SPD in PBS (pH7.4) was immobilized on an Amine Reactive 2nd Generation (AR2G) sensor (Fortebio). Purified $HADHA_2$ protein was diluted in PBS (pH 7.4) / 0.04% Tween / 0.01% BSA (kinetics buffer) to a concentration of 15 nM. The kinetics buffer was used as a running buffer in all data acquisition steps. Actual binding to SPD was obtained by subtracting nonspecific binding to a reference sensor (no SPD immobilized) from total binding to the SPD sensor. K_D, k_{on}, and k_{off} values were calculated and fitted by the Octet Data Analysis 8.1 Software (Fortebio). 1:2 bivalent binding model gave the best fit between the theoretical values and the actual measurement. Kinetic constants were determined by integrating the experimental data using the differential rate equation $dR / dt = k_{on} \cdot C \cdot (Rmax - R) - k_{dis} \cdot R$ to obtain k_{on} and k_{off} values simultaneously (R = observed response, Rmax = maximum response upon saturation, C = analyte concentration, k_{on} = association rate constant, k_{off} = dissociation rate constant). Then, the ratio between k_{dis} and k_{off} gives the reported dissociation constants (K_D). The goodness of fit was evaluated by the reduced chi-square ($\chi 2$) and the R2 value.

Immunofluorescent staining of HDAHA and HADHB

For immunostaining of HDAHA and HADHB, Jurkat cells were fixed with 4% paraformaldehyde in phosphate buffer solution (09154-85, Nacalai Tesque) for 15 min and washed three times with fluorescence-activated cell sorting (FACS) buffer. Briefly, cells were permeabilized using 0.5% TritonX-100 buffer (10 mM Tris HCl, 50 mM NaCl, 5 mM EDTA, 0.02% NaN_3, and 0.5% TrotonX-100) for 10 min and washed three times with FACS buffer (10% FCS in PBS). Cells were then incubated with anti-HADHA/HADHB antibody (1:100 dilution in FACS buffer, ab110302, abcam). One hour after the primary antibody incubation, cells were washed three times with FACS buffer and incubated with FITC conjugated anti-mouse IgG antibody (1:100 dilution in FACS buffer, 103002, SouthernBiotech) for 1.5 hours at room temperature in the dark. After washing with FACS buffer, immunofluorescence images were collected using Olympus SpinSR10 spining disk confocal super-resolution microscope high-sensitivity model (×100 magnification).

Duolink in situ PLA

Jurkat cells were cultured with or without SPD (0.2 μM) for 2 days. To detect interaction between SPD and HADHA/HADHB by Duolink analysis (*46*), fixation and permiabilization were performed as described in immunofluorescent part. Cells were then subjected to anti-HADHA/HADHB antibody (1:100; ab110302, abcam) and rabbit anti-SPD antibody (1:300; abcam, ab7318). According to manufacturer's instructions, the hybridization reaction between oligonucleotide conjugated to 2nd mAb (Sigma-Aldaich, anti-mouse DUO92001 for HADHA/HADHB and anti-rabbit DUO92006 for SPD) and PLA probes were amplified with DNA polymerase. The signals were detected by Duolink in situ detection reagent orange (Sigma-Aldaich, DUO92007). Cells were mounted onto slides using Vactashield mounting medium with DAPI (Vector laboratories, Inc.) and images were taken using Olympus SpinSR10 confocal microscope (×100 magnification).

Recombinant MTP protein expression and purification

Construction of the expression plasmid for human HADHA (also known as MTPα subunit) and human HADHB (MTPβ subunit) was based on the backbone of the *E. coli* plasmid pET-21b (+) and pET-28a (+), respectively. For expression of the MTP in the $\alpha_2\beta_2$-heterotetrameric form, the tag-free HADHA (UniProt ID: P40939, residues 37 to 763) was inserted downstream of the T7 promoter of pET-21b (+). The HADHB (UniProt ID: P55084, residues 34 to 474) was fused with a His_8 tag at the N terminus and inserted downstream of the T7 promoter of pET-28a (+). *E. coli* Rosetta (DE3) cells (Novagen) were transformed with the resulting two plasmids. The transformants were selected on LB plates supplemented with 100 mg/liter ampicillin and 50 mg/liter kanamycin. For purification of HADHA alone in the α_2 form, the HADHA was fused with a His_8 tag at the N terminus and inserted downstream of the T7 promoter of pET-21b (+). This was followed by *E. coli* Rosetta (DE3) transformation and selection on LB plates supplemented with 100 mg/liter ampicillin. All of the cloned inserts were verified by sequencing both strands.

E. coli Rosetta (DE3) cells harboring the two expression plasmids for MTP were grown overnight at 37°C and 250 rpm in LB supplemented with 100 mg/liter ampicillin and 50 mg/liter kanamycin. The culture was diluted 1:100 into the same medium and grown at 37°C to an OD_{600} of 0.7 followed by overnight incubation at 23°C with 0.1 mM IPTG. The cells were harvested by centrifugation at 6000 g for 15 min and re-suspended in buffer A (100 mM Tris-HCl, pH 8.0, 200 mM NaCl, Roche EDTA-free protease inhibitor tablet). Cells were disrupted by several cycles of sonication on ice for 10 min. The membranes were isolated by ultracentrifugation at 45,000 rpm for 30 min, homogenized in buffer A supplemented with 40% glycerol, frozen in liquid nitrogen and stored at −80°C. For MTP purification, membrane extraction from 16 liters of culture was used for each batch of preparation. Membranes were solubilized with 1% DDM in buffer B (50 mM HEPES-NaOH, pH 7.5, 150 mM NaCl, 20 mM imidazole, 1 mM EDTA, 10% glycerol). After ultracentrifugation for 30 min at 45,000 rpm, the supernatant was loaded onto a 5-ml HisTrap Crude column (Cytiva) equilibrated with buffer C (100 mM Tris-HCl, pH 8.0, 200 mM NaCl, 0.02% DDM, 20 mM imidazole). A linear gradient of 20 to 500 mM imidazole was used for elution. The MTP fractions were collected, concentrated and loaded onto a Superdex 200 Increase 10/300 GL gel filtration column (Cytiva) equilibrated with buffer D (20 mM potassium phosphate buffer, pH 7.7, 100 mM NaCl, 0.02% DDM). The peak fractions were pooled, concentrated using an Amicon Ultra-4 spin filter (MWCO 50 K; Millipore) and used for enzymological and ligand-binding studies without freezing. The same purification method was used for the HADHA alone in the α_2 form.

Coimmunoprecipitation of SPD-conjugated MTP by anti-SPD antibody

Purified MTP was incubated with or without SPD (5 mM) and then immunoprecipitated with anti-SPD antibody (abcam, ab7318)–coated Dynabeads Protein G (Invitrogen). After incubation for overnight at 4°C on a rotator, the beads were washed three times using 10 times diluted buffer D (20 mM potassium phosphate buffer, pH 7.7, 100 mM NaCl, 0.02% DDM) in 100 mM Tris-HCl (pH 7.5). To elute precipitated proteins, the beads were incubated for 1 hour at 4°C with 5 mM SPD in the same buffer as described above except containing 0.1% NP-40. The eluted proteins were separated in

4 to 20% Mini-PROTEAN TGX Precast gels (Bio-Rad) for SDS-PAGE and transferred to Immobilon-P membranes (Millipore). For the detection of HADHA and HADHB bands, the anti-HADHA/HADHB (1/500, ab110302, abcam) mAb used in PLA assays and mouse IgG HRP (1/20000,18-8817-33, Rockland) were used. Membranes were blocked with 4% (w/v) nonfat dry milk for 30 min at room temperature and then incubated with primary antibodies for 3 hours at room temperature. Then, secondary antibodies conjugated to horseradish peroxidase (HRP) were incubated for 1 hour at room temperature. Proteins were detected by Chemilumi One Super (Nacalai Tesque).

MTP enzyme activities

3-hydroxyacyl-CoA dehydrogenase assay

The activity of HADHA subunit of MTP was evaluated as a measurement of change in the concentration of NADH. The assay buffer is composed of 50 mM of Tris-HCl (pH 7.5), 1 mM of EDTA (pH 7.5), 250 μM (or as specified) of NADH, and 100 μM of acetoacetyl CoA. In 180 μl of assay buffer, 10 μl of MTP enzyme (containing 0.5 to 0.7 μg) and 10 μl of SPD were added, and the change in NADH concentration was monitored by the absorbance decrease at 340 nm at room temperature (24° to 25°C) every 1 min for 20 min. To obtain the enzymatic activity graphs and K_m values, the data after 10 min were used. The value at each point was adjusted so that the value of the respective controls comes to 0. The control in SPD affinity to MTP experiments is 0 μM SPD and in NADH affinity experiments is 0 μM MTP.

3-ketoacyl-CoA thiolase assay

The activity of the HADHB subunit of MTP was evaluated as a measurement of change in the concentration of acetoacetyl CoA. The assay buffer is composed of 100 mM of Tris-HCl (pH 7.5), 25 mM of $MgCl_2$, and 100 μM (or as specified) of acetoacetyl CoA. In 180 μl of assay buffer, 10 μl of MTP enzyme (containing 1 to 2 μg) and 10 μl of SPD were added. The change in acetoacetyl CoA concentration was monitored by the absorbance decrease at 303 nm at 30°C every 1 min for 20 min. To obtain the enzymatic activity graphs and K_m values, the data after 10 min were used. The value at each point was adjusted so that the value of respective experimental controls comes to 0. The control in SPD affinity to MTP experiments is 0 μM SPD and in acetoacetyl CoA affinity experiments is 0 μM MTP.

Flow cytometry analysis

The following monoclonal antibodies recognizing the indicated antigens were used: CD8 (53-6.7), CD45.2 (104), CD44 (1M7), CD62L (MEL14), CD4 (RM4-5), Foxp3 (FJK-16s), F4/80 (BM8), and Arg1 (A1exF5) from eBioscience; PD-1 (RMP1-30), Tim-3 (RMT3-23), granzyme b (QA16A02), CD49b (DX5), and CD11b (M1/70) from Biolegend; and MHCII (M5/114.15.2) and MHCI (AF6-88.5) from BD bioscience. For cell surface staining, 2×10^5 cell pellets were stained with appropriately diluted antibodies for 12 min in 4°C. Cells were washed by 10% FCS PBS and run. To measure intracellular granzyme B production, cells were stimulated with PMA and ionomycin (Sigma-Aldrich) in the presence of GolgiStop (BD Biosciences) for 4 hours. Intracellular staining was performed using Fixation/Permeabilization Solution Kit (BD Biosciences). All flow cytometry experiments were performed on a FACSCanto II (BD Biosciences) or LSR Fortessa X-20 (BD Biosciences) and analyzed using FlowJo software.

Transmission electron microscopy (TEM)

For TEM observation, treated cells were embedded in iPGell (GenoStaff) according to the manufacturer's instructions. The cell blocks were fixed with 4% formaldehyde and 2% glutaraldehyde in 0.1 M phosphate buffer (PB) (pH 7.4) overnight at 4°C, then postfixed with 1% O_SO_4 in 0.1M PB for 2 hours. After dehydration in a series of graded concentrations of ethanol, the fixed cell blocks were embedded in epoxy resin (Luveak 812; Nacalai Tesque). Ultrathin sections (70-nm thickness) were prepared on an ultramicrotome (EM UC6; Leica). The sections were then stained with uranyl acetate and lead citrate and finally examined with an electron microscope (H-7650 Hitachi Tokyo). TEM was performed at the Division of Electron Microscopic Study, Center for Anatomical Studies, Graduate School of Medicine, Kyoto University.

CPT1a knock down by CRISPR interference system in Jurkat

Jurkat cells were transfected with pLKO5d. SFFV.dCas9-KRAB.P2A.BSD using FuGENE 6 (E2691, Promega) and selected with blasticidin (*47*). The PB-Human CPT1a oligo#1-Puro was transfected by electroporation with Cell Line NucleofectorTM Kit V (Lonza VCA-1003). The guide RNA sequence of human CPT1a oligo#1 was as follows

Human CPT1a -1F: 5′- CACC AGGCC-GAGCGCACCCGACGC - 3′

Human CPT1a -1R: 5′- AAAC GCGTCGGGTGCGCTCGGCCT - 3′

Statistical analysis

Statistical analysis was performed using Prism 8 (GraphPad Software). For multiple-group analysis, one- or two-way analysis of variance (ANOVA) followed by Sidak's multiple comparisons test or column factor comparison were used to analyze, focusing on the main groups. To compare two groups, the two-tailed unpaired Student's *t* test or unpaired multiple *t* test were used. To assess the statistical significance in survival curves, we used the Mantel-Cox test. All statistical tests were two-tailed, assume parametric data accordingly, and a *P* value of ≦0.05 was considered significant. The variations of data were evaluated as the means, standard errors of the mean (SEMs), or standard deviations (SDs). Three or more samples were thought to be appropriate for the sample size estimate in this study. In some cases, cells were pooled from multiple mice in one experiment. Samples and animals were randomly chosen from the pool and treated. No blinding method was used for the treatment of samples and animals.

REFERENCES AND NOTES

1. R. H. Houtkooper *et al*., The metabolic footprint of aging in mice. *Sci. Rep.* **1**, 134 (2011). doi: 10.1038/srep00134; pmid: 22355651
2. R. Sharma, A. Ramanathan, The Aging Metabolome—Biomarkers to Hub Metabolites. *Proteomics* **20**, 1800407 (2020). doi: 10.1002/pmic.201800407; pmid: 32068959
3. V. Azzu, T. G. Valencak, Energy Metabolism and Ageing in the Mouse: A Mini-Review. *Gerontology* **63**, 327–336 (2017). doi: 10.1159/000454924; pmid: 28118636
4. F. Madeo, T. Eisenberg, F. Pietrocola, G. Kroemer, Spermidine in health and disease. *Science* **359**, eaan2788 (2018). doi: 10.1126/science.aan2788; pmid: 29371440
5. T. Eisenberg *et al*., Induction of autophagy by spermidine promotes longevity. *Nat. Cell Biol.* **11**, 1305–1314 (2009). doi: 10.1038/ncb1975; pmid: 19801973
6. Y. Nakajima, K. Chamoto, T. Oura, T. Honjo, Critical role of the $CD44^{low}CD62L^{low}$ $CD8^+$ T cell subset in restoring antitumor immunity in aged mice. *Proc. Natl. Acad. Sci. U.S.A.* **118**, e2103730118 (2021). doi: 10.1073/pnas.2103730118; pmid: 34088845
7. G. Alsaleh *et al*., Autophagy in T cells from aged donors is maintained by spermidine and correlates with function and vaccine responses. *eLife* **9**, e57950 (2020). doi: 10.7554/eLife.57950; pmid: 33317695
8. K. Araki *et al*., mTOR regulates memory CD8 T-cell differentiation. *Nature* **460**, 108–112 (2009). doi: 10.1038/nature08155; pmid: 19543266
9. E. L. Pearce *et al*., Enhancing CD8 T-cell memory by modulating fatty acid metabolism. *Nature* **460**, 103–107 (2009). doi: 10.1038/nature08097; pmid: 19494812
10. M. D. Buck, D. O'Sullivan, E. L. Pearce, T cell metabolism drives immunity. *J. Exp. Med.* **212**, 1345–1360 (2015). doi: 10.1084/jem.20151159; pmid: 26261266
11. E. Morselli *et al*., Spermidine and resveratrol induce autophagy by distinct pathways converging on the acetylproteome. *J. Cell Biol.* **192**, 615–629 (2011). doi: 10.1083/jcb.201008167; pmid: 21339330
12. M. H. Park, E. C. Wolff, Hypusine, a polyamine-derived amino acid critical for eukaryotic translation. *J. Biol. Chem.* **293**, 18710–18718 (2018). doi: 10.1074/jbc.TM118.003341; pmid: 30257869
13. Y. Liang *et al*., eIF5A hypusination, boosted by dietary spermidine, protects from premature brain aging and mitochondrial dysfunction. *Cell Rep.* **35**, 108941 (2021). doi: 10.1016/j.celrep.2021.108941; pmid: 33852845
14. D. J. Puleston *et al*., Polyamine metabolism is a central determinant of helper T cell lineage fidelity. *Cell* **184**, 4186–4202.e20 (2021). doi: 10.1016/j.cell.2021.06.007; pmid: 34216540
15. M. T. Hyvönen *et al*., Role of hypusinated eukaryotic translation initiation factor 5A in polyamine depletion-induced cytostasis. *J. Biol. Chem.* **282**, 34700–34706 (2007). doi: 10.1074/jbc.M704282200; pmid: 17901051
16. G. M. Carriche *et al*., Regulating T-cell differentiation through the polyamine spermidine. *J. Allergy Clin. Immunol.* **147**, 335–348.e11 (2021). doi: 10.1016/j.jaci.2020.04.037; pmid: 32407834
17. Q. Yang *et al*., Spermidine alleviates experimental autoimmune encephalomyelitis through inducing inhibitory macrophages. *Cell Death Differ.* **23**, 1850–1861 (2016). doi: 10.1038/cdd.2016.71; pmid: 27447115

18. N. Patsoukis *et al*., PD-1 alters T-cell metabolic reprogramming by inhibiting glycolysis and promoting lipolysis and fatty acid oxidation. *Nat. Commun.* **6**, 6692 (2015). doi: 10.1038/ncomms7692; pmid: 25809635
19. P. S. Chowdhury, K. Chamoto, A. Kumar, T. Honjo, PPAR-Induced Fatty Acid Oxidation in T Cells Increases the Number of Tumor-Reactive CD8$^+$ T Cells and Facilitates Anti–PD-1 Therapy. *Cancer Immunol. Res.* **6**, 1375–1387 (2018). doi: 10.1158/2326-6066.CIR-18-0095; pmid: 30143538
20. V. Kalia *et al*., Metabolic regulation by PD-1 signaling promotes long-lived quiescent CD8 T cell memory in mice. *Sci. Transl. Med.* **13**, eaba6006 (2021). doi: 10.1126/scitranslmed.aba6006; pmid: 34644150
21. K. Chamoto *et al*., Mitochondrial activation chemicals synergize with surface receptor PD-1 blockade for T cell-dependent antitumor activity. *Proc. Natl. Acad. Sci. U.S.A.* **114**, E761–E770 (2017). doi: 10.1073/pnas.1620433114; pmid: 28096382
22. D. A. Ferrick, A. Neilson, C. Beeson, Advances in measuring cellular bioenergetics using extracellular flux. *Drug Discov. Today* **13**, 268–274 (2008). doi: 10.1016/j.drudis.2007.12.008; pmid: 18342804
23. P. Marchetti, Q. Fovez, N. Germain, R. Khamari, J. Kluza, Mitochondrial spare respiratory capacity: Mechanisms, regulation, and significance in non-transformed and cancer cells. *FASEB J.* **34**, 13106–13124 (2020). doi: 10.1096/fj.202000767R; pmid: 32808332
24. G. J. van der Windt *et al*., Mitochondrial respiratory capacity is a critical regulator of CD8$^+$ T cell memory development. *Immunity* **36**, 68–78 (2012). doi: 10.1016/j.immuni.2011.12.007; pmid: 22206904
25. B. Raud *et al*., Etomoxir Actions on Regulatory and Memory T Cells Are Independent of Cpt1a-Mediated Fatty Acid Oxidation. *Cell Metab.* **28**, 504–515.e7 (2018). doi: 10.1016/j.cmet.2018.06.002; pmid: 30043753
26. D. J. Puleston *et al*., Polyamines and eIF5A Hypusination Modulate Mitochondrial Respiration and Macrophage Activation. *Cell Metab.* **30**, 352–363.e8 (2019). doi: 10.1016/j.cmet.2019.05.003; pmid: 31130465
27. K. Liang *et al*., Cryo-EM structure of human mitochondrial trifunctional protein. *Proc. Natl. Acad. Sci. U.S.A.* **115**, 7039–7044 (2018). doi: 10.1073/pnas.1801252115; pmid: 29915090
28. C. Xia, Z. Fu, K. P. Battaile, J. P. Kim, Crystal structure of human mitochondrial trifunctional protein, a fatty acid β-oxidation metabolon. *Proc. Natl. Acad. Sci. U.S.A.* **116**, 6069–6074 (2019). doi: 10.1073/pnas.1816317116; pmid: 30850536
29. M. M. Adeva-Andany, N. Carneiro-Freire, M. Seco-Filgueira, C. Fernández-Fernández, D. Mouriño-Bayolo, Mitochondrial β-oxidation of saturated fatty acids in humans. *Mitochondrion* **46**, 73–90 (2019). doi: 10.1016/j.mito.2018.02.009; pmid: 29551309
30. A. M. Rahul, K. Sasaki, K. Titani, M. Miyazaki, Biochemical and immunological characterization of deoxyhypusine synthase purified from the yeast *Saccharomyces carlsbergensis*. *J. Biochem.* **121**, 769–778 (1997). doi: 10.1093/oxfordjournals.jbchem.a021652; pmid: 9163530
31. F. Pietrocola *et al*., Spermidine induces autophagy by inhibiting the acetyltransferase EP300. *Cell Death Differ.* **22**, 509–516 (2015). doi: 10.1038/cdd.2014.215; pmid: 25526088
32. M. Bagherniya, A. E. Butler, G. E. Barreto, A. Sahebkar, The effect of fasting or calorie restriction on autophagy induction: A review of the literature. *Ageing Res. Rev.* **47**, 183–197 (2018). doi: 10.1016/j.arr.2018.08.004; pmid: 30172870
33. I. Guerrero-Ros *et al*., The negative effect of lipid challenge on autophagy inhibits T cell responses. *Autophagy* **16**, 223–238 (2020). doi: 10.1080/15548627.2019.1606635; pmid: 30982401
34. Y. Xie, J. Li, R. Kang, D. Tang, Interplay Between Lipid Metabolism and Autophagy. *Front. Cell Dev. Biol.* **8**, 431 (2020). doi: 10.3389/fcell.2020.00431; pmid: 32582708
35. F. Pietrocola *et al*., Caloric Restriction Mimetics Enhance Anticancer Immunosurveillance. *Cancer Cell* **30**, 147–160 (2016). doi: 10.1016/j.ccell.2016.05.016; pmid: 27411589
36. L. Ma *et al*., Spermidine ameliorates high-fat diet-induced hepatic steatosis and adipose tissue inflammation in preexisting obese mice. *Life Sci.* **265**, 118739 (2021). doi: 10.1016/j.lfs.2020.118739; pmid: 33186567
37. M. Hargreaves, L. L. Spriet, Skeletal muscle energy metabolism during exercise. *Nat. Metab.* **2**, 817–828 (2020). doi: 10.1038/s42255-020-0251-4; pmid: 32747792
38. M. Knobloch *et al*., A Fatty Acid Oxidation-Dependent Metabolic Shift Regulates Adult Neural Stem Cell Activity. *Cell Rep.* **20**, 2144–2155 (2017). doi: 10.1016/j.celrep.2017.08.029; pmid: 28854364
39. D. Shao *et al*., Increasing Fatty Acid Oxidation Prevents High-Fat Diet-Induced Cardiomyopathy Through Regulating Parkin-Mediated Mitophagy. *Circulation* **142**, 983–997 (2020). doi: 10.1161/CIRCULATIONAHA.119.043319; pmid: 32597196
40. K. Tanigaki *et al*., Regulation of αβ/γδ T cell lineage commitment and peripheral T cell responses by Notch/RBP-J signaling. *Immunity* **20**, 611–622 (2004). doi: 10.1016/S1074-7613(04)00109-8; pmid: 15142529
41. A. Kumar, K. Chamoto, P. S. Chowdhury, T. Honjo, Tumors attenuating the mitochondrial activity in T cells escape from PD-1 blockade therapy. *eLife* **9**, e52330 (2020). doi: 10.7554/eLife.52330; pmid: 32122466
42. M. Ishida *et al*., Differential expression of PD-L1 and PD-L2, ligands for an inhibitory receptor PD-1, in the cells of lymphohematopoietic tissues. *Immunol. Lett.* **84**, 57–62 (2002). doi: 10.1016/S0165-2478(02)00142-6; pmid: 12161284
43. L. Reiter *et al*., mProphet: Automated data processing and statistical validation for large-scale SRM experiments. *Nat. Methods* **8**, 430–435 (2011). doi: 10.1038/nmeth.1584; pmid: 21423193
44. G. Rosenberger *et al*., Statistical control of peptide and protein error rates in large-scale targeted data-independent acquisition analyses. *Nat. Methods* **14**, 921–927 (2017). doi: 10.1038/nmeth.4398; pmid: 28825704
45. M. Miyajima *et al*., Metabolic shift induced by systemic activation of T cells in PD-1-deficient mice perturbs brain monoamines and emotional behavior. *Nat. Immunol.* **18**, 1342–1352 (2017). doi: 10.1038/ni.3867; pmid: 29058703
46. M. S. Alam, Proximity Ligation Assay (PLA). *Curr. Protoc. Immunol.* **123**, e58 (2018). doi: 10.1002/cpim.58; pmid: 30238640
47. A. Schwarzer *et al*., The non-coding RNA landscape of human hematopoiesis and leukemia. *Nat. Commun.* **8**, 218 (2017). doi: 10.1038/s41467-017-00212-4; pmid: 28794406

ACKNOWLEDGMENTS

We sincerely thank Y. Kitawaki, A. Kumar, M. Akrami, R. Hatae, P. Chowdhury, M. Demir, T. Hirano, Y. Zou, K. Yamasaki, E. Mohemad, W. Yu, K. Ito, J. Wang, T. Oura, and M. Hajime-Sumikawa for assistance with sample preparation and useful discussion.
Funding: This work was supported by the Japan Agency for Medical Research and Development (AMED) under grant nos. 20cm0106302 (T.H.), 19gm0710012 (S.F.), 19gm0810001 (T.O.), and JP21zf0127004 and 22ama221305 (K.C.); the Ministry of Education, Culture, Sports, Science and Technology–Japan (MEXT) under grant no. 150709 (M.A.-H.); Grant-in-aid Scientific Research (B) under grant nos. 21H03087 (K.C.) and 18H02425 (Y.W.); the Tang Prize Foundation (T.H.); the Yanai Fund (T.H.); 2019 Bristol-Myers Squibb Research Grants (K.C.); the RIKEN Aging Project grant (S.F.); Meiji Holdings Co., Ltd. (T.H.); Meiji Seika Pharma Co., Ltd. (T.H.); and the Bristol-Myers Squibb Company (T.H.). **Author contributions:** M.A.-H., K.C., T.O., S.F., and T.H. designed the research; M.A.-H., K.C., T.O., K.S., N.N., A.M., Y.W., R.M., B.Z., Y.Na., K.M., Y.S., T.M., K.K., Y.H., S.D., K.Y., and Y.No. performed research; M.A.-H., K.C., T.O., N.N., F.M., and S.I. analyzed data; and M.A.-H., K.C., S.F., and T.H. wrote the paper. **Competing interests:** T.H. received research grants from Meiji Holdings Co., Ltd., Meiji Seika Pharma, and Bristol-Myers Squibb Company for this study. T.H., K.C., and S.F. are inventors on a patent (PCT/JP2020/041190) submitted by Kyoto University and RIKEN that covers combination therapy of PD-1 blockade therapy and SPD. The authors declare no other competing interests. **Data and materials availability:** All of the proteomics data (protein expression data) generated in this study have been deposited in Proteomexchange database (http://www.proteomexchange.org/) with accession no. PXD036425. All other data are available in the manuscript or the supplementary materials.

SUPPLEMENTARY MATERIALS

science.org/doi/10.1126/science.abj3510
Figs. S1 to S11
MDAR Reproducibility Checklist

View/request a protocol for this paper from *Bio-protocol*.

Submitted 7 May 2021; resubmitted 21 February 2022
Accepted 29 September 2022
10.1126/science.abj3510

Spermidine activates mitochondrial trifunctional protein and improves antitumor immunity in mice

Muna Al-HabsiKenji ChamotoKen MatsumotoNorimichi NomuraBaihao ZhangYuki SugiuraKazuhiro SonomuraAprilia MaharaniYuka NakajimaYibo WuYayoi NomuraRosemary MenziesMasaki TajimaKoji KitaokaYasuharu HakuSara DelghandiKeiko YurimotoFumihiko MatsudaSo IwataToshihiko OguraSidonia FagarasanTasuku Honjo

Science, 378 (6618), eabj3510. • DOI: 10.1126/science.abj3510

Spermidine fights cancer in aging mice

Abundance of the polyamine spermidine decreases in aging mice, and supplementation can have restorative effects and extend life span. Al-Habsi *et al*. explored whether loss of spermidine might contribute to loss of antitumor immunity in aged mice. Restoration of spermidine concentrations enhanced antitumor responses stimulated by programmed death ligand-1 (PD-L1) monoclonal antibody therapy. Spermidine appeared to directly affect T cell function by increasing fatty acid oxidation. Tagged spermidine bound to components of the mitochondrial trifunctional protein complex, thus increasing fatty acid oxidation and the production of ATP. The authors propose that these effects may contribute to the effects of spermidine in promoting longevity. —LBR